NASA TECHNICAL NOTE

NASA TN D-7211

NASA TN D-7211

THE EFFECT OF FINITE THRUST AND HEATING CONSTRAINTS ON THE SYNERGETIC PLANE CHANGE MANEUVER FOR A SPACE SHUTTLE ORBITER-CLASS VEHICLE

by E. D. Dickmanns

George C. Marshall Space Flight Center
Marshall Space Flight Center, Ala. 35812

NATIONAL AERONAUTICS AND SPACE ADMINISTRATION • WASHINGTON, D. C. • OCTOBER 1973

TECHNICAL REPORT STANDARD TITLE PAGE

1. REPORT NO.	2. GOVERNMENT ACCESSION NO.	3. RECIPIENT'S CATALOG NO.
NASA TN D-7211		

4. TITLE AND SUBTITLE	5. REPORT DATE
The Effect of Finite Thrust and Heating Constraints on the Synergetic Plane Change Maneuver for a Space Shuttle Orbiter-Class Vehicle	October 1973
	6. PERFORMING ORGANIZATION CODE
7. AUTHOR(S) E. D. Dickmanns	8. PERFORMING ORGANIZATION REPORT # M105
9. PERFORMING ORGANIZATION NAME AND ADDRESS George C. Marshall Space Flight Center Marshall Space Flight Center, Alabama 35812	10. WORK UNIT NO.
	11. CONTRACT OR GRANT NO.
	13. TYPE OF REPORT & PERIOD COVERED
12. SPONSORING AGENCY NAME AND ADDRESS National Aeronautics and Space Administration Washington, D.C. 20546	Technical Note
	14. SPONSORING AGENCY CODE

15. SUPPLEMENTARY NOTES
Prepared by Aero-Astrodynamics Laboratory,
Science and Engineering

16. ABSTRACT

Numerical solutions to the optimal three-dimensional glide/thrust atmosphere skip maneuver are obtained using the multiple shooting iteration scheme. A singular thrust arc, induced by the heating constraints, is encountered. The synergetic plane change maneuver is shown to be superior to an extra-atmospheric one for 556-km (300-nm) circular orbit plane changes of more than 5 degrees.

NOTE: This research was performed under postdoctoral research associateship sponsored by the National Academy of Sciences while the author was on leave from the Deutsche Forschungs-und Versuchsanstalt für Luft- und Raumfahrt, Oberpfaffenhofen, Germany.

17. KEY WORDS	18. DISTRIBUTION STATEMENT
Orbit transfer Optimization Entry Trajectories	Unclassified - Unlimited E. D. Geissler, Director Aero-Astrodynamics Laboratory

19. SECURITY CLASSIF. (of this report)	20. SECURITY CLASSIF. (of this page)	21. NO. OF PAGES	22. PRICE
Unclassified	Unclassified	45	Domestic, $3.00 Foreign, $5.50

For sale by National Technical Information Service, Springfield, Virginia 22151

TABLE OF CONTENTS

LIST OF ILLUSTRATIONS

DEFINITION OF SYMBOLS

Symbol	Definition
B_i	Coefficients in heating constraint representation
b	Mass flow rate or constant in heating constraint (meaning obvious from context)
C_i	Coefficients in heating constraint representation
C	Constraint function
C_D	Drag coefficient
C_{Do}	Drag coefficient for zero lift
C_L	Lift coefficent
C_{LH}	Lift coefficient determined from heating constraint
ΔC_{LH}	Adjustment parameter in heating constraint representation
D	Drag force
F	Aerodynamic reference area
f	Vector of right side of differential equations
$G_{i,j}$	Coefficient matrix for bivariate heating constraint
g	Gravitational acceleration
H_i	Coefficients in heating constraint representation
H	Hamiltonian function
h	Altitude
K	Abbreviation, equation (42)
k	Factor in lift dependent drag term
L	Aerodynamic lift force
m	Vehicle mass
n	Exponent in lift dependent drag term

DEFINITION OF SYMBOLS (Continued)

Symbol	Definition
q	Dynamic pressure $0.5\,\rho V^2$
R_o	Earth radius
r	Radius vector to vehicle c.g.
S_T	Thrust switching function
T	Thrust force
t	Time
U_e	Jet exit velocity
u	Controls, 5-vector $u^T = (C_L, \mu, b, \epsilon, \sigma)$
v	Velocity
w	Square root expressions in optimal control
X	State vector $X^T = (v, \chi, \gamma, \Lambda, h, m)$ general coordinate
α	Angle of attack
β	Inverse scale height of atmosphere
Γ	Gravitational constant times planet mass
γ	Flight path angle
ϵ	Out of vertical plane thrust angle
ϕ	Heating constraint function
$\circledcirc$	Downrange angle
Λ	Crossrange angle
λ	Lagrangian multipliers, costate variables (subscripted by corresponding state variable symbol)

DEFINITION OF SYMBOLS (Concluded)

Symbol	Definition
μ	Aerodynamic bank angle
χ	Heading angle
ρ	Air density
ρ_o	Air density at sea level
σ	Thrust angle in vertical plane
Indices	
a	Aerodynamic
c	Constrained
e	Entry condition
f	Exit condition
p	Perigee
S	Corresponding to circular satellite orbit
T	Thrust related
uc	Unconstrained

THE EFFECT OF FINITE THRUST AND HEATING CONSTRAINTS ON THE SYNERGETIC PLANE CHANGE MANEUVER FOR A SPACE SHUTTLE ORBITER-CLASS VEHICLE

INTRODUCTION

In the synergetic plane change maneuver, propulsive and aerodynamic forces are used in conjunction to achieve a rotation of the orbital plane by dipping into a planetary atmosphere using the lift to effect part of the plane change, the thrust providing the rest and adding the lost energy due to drag. Several special maneuvers have been discussed in the literature since 1962 [1-18]. A survey over these has been given in Reference 19. In all investigations, the total maneuver has been broken down into deboost, descent, atmospheric/thrusting flight, ascent, and injection into the new orbit. To narrow the field of parameters, mainly plane changes of circular orbits have been considered. The phases mentioned above were investigated separately and later pieced together, yielding only rough estimates of the total performance achievable.

In References 19 and 20, a variational formulation for the atmospheric skip phase was given and analytical approximate and numerical results for unconstrained maneuvers and the effect of a normal acceleration constraint were presented. The deboost phase and the ascent burn phase were considered to be impulsive which together with information from the aerodynamic glide phase allowed an approximate determination of favorable interface parameter between these phases. Especially, ascent thrust angles and thrusting altitudes were obtained from simple function minimizations. Kinetic heating considerations had not been considered since the estimation of a lower limit for the ΔV requirement was the primary purpose of the investigation. The resulting aerodynamic skips showed high heating and acceleration peaks, especially for larger plane change angles which desired steep entry flight path angles.

For a realistic maneuver with state-of-the-art materials, a heating constraint has to be considered which is more severe than the normal acceleration constraints considered in References 19 and 20. This type of performance reduction caused by the vehicle skin temperature limitation has been investigated by Clauss and Yeatman [12] for a minor circle glide turn and a steady state aerocruise maneuver. They concluded that the temperature constraint is more detrimental to the glide than to the aerocruise maneuver.

The objective of this report is to investigate the effect of a heating limit on a finite thrust optimal plane change maneuver for a Space Shuttle orbiter-type vehicle. Only the central portion of the maneuver (Fig. 1) which lies in the dense atmosphere is considered; this, however, is a full variational formulation. The remaining mass fraction after the burn phases is being maximized. Numerical result for a limited range of parameters will be given. They were obtained partly by a refined gradient optimization program and partly by a multiple shooting algorithm to solve the boundary value problem resulting from the application of the maximum principle.

MATHEMATICAL MODEL

To keep the computational work load in this exploratory study low, a relatively simple process model has been adopted which is described in this section.

Planet Characteristics

The planet is assumed to be a nonrotating sphere with a stationary atmosphere independent of geographical coordinates. No winds are assumed and the density altitude relationship is exponential

$$\rho = \rho_0 \exp(-\beta h) \tag{1}$$

where β is the inverse scale height $\beta = 1.0/6.9$ [km^{-1}] and ρ_0 is the density at sea level $\rho_0 = 1.54$ [kg/m^3] for earth.

An inverse square gravity law

$$g = \Gamma/r^2 \tag{2}$$

$$r = R_0 + h \tag{3}$$

with sea level radius $R_0 = 6371.2$ km for earth and Γ = gravitational constant times planet mass (3.986×10^{14} m^3/s^2 for earth) were considered a good approximation.

The neglection of the planet rotation results in large errors in the heating equations for equatorial entry, where, for earth the velocity increment caused by rotation is 6 percent of the satellite velocity resulting in about 20-percent heating rate error. Therefore, the results presented correspond more to a meridional entry in higher latitudes. Viscous interaction effects at high altitudes are neglected, leading to a constant hypersonic drag polar for the vehicle.

Vehicle Model

The drag polar was chosen as a constant medium one for the altitude range of the maneuver and represented by

$$C_D = C_{Do} + k\, C_L^{\,n} \tag{4}$$

where C_{Do} is the zero lift drag coefficient and n is the power of the lift-dependent drag (actual values: C_{Do} = 0.04, k = 1.0, and n = 1.86, resulting in a maximum L/D of 2.22 for C_{LE} = 0.192). The considerable influence of viscous interaction effects on the optimal aerodynamic control for the unconstrained synergetic maneuver has been shown in References 19 and 20. The effect on the performance, however, was only minor.

The second important aerodynamic parameter is the wing loading. Low values lead to higher skipping altitudes and lower heating loads while the vehicle has to be larger for the same payload. A value of m_o/F = 275 [kg/m^2] was chosen as nominal; the effect of increasing it to 300 kg/m^2 was determined by one sensitivity test run. No aerodynamic side forces were considered assuming that the sideslip angle is always zero.

A chemical propulsion system with unconstrained thrust direction was assumed without atmospheric back-pressure losses

$$\frac{T}{m_o} = b \cdot U_e \quad . \tag{5}$$

The exit velocity U_e was chosen to be U_e = 4.36 [km/s] and the relative mass flow rate $b \approx 0.002$ [s^{-1}], resulting in an initial thrust acceleration of about 1 g_o.

Heating Constraint

The heating constraint for a reentry vehicle is one of the driving factors in trajectory shaping. Medium- (like the proposed Space Shuttle orbiter) and high-L/D vehicles have a thermal protection system (TPS) consisting of reradiative and ablative elements at different parts of the vehicle [21]. The higher the L/D, the more reradiative the TPS is going to be. If the time constants for the outer skin to heat up to the design limit is small compared to the rate at which the vehicle state (especially altitude, angle of attack, and velocity) changes, then a quasisteady approximation is valid. In this case, the heating constraint can be formulated as an algebraic equation $\phi(v, h, \alpha) = 0$, where v is the aerodynamic velocity, h is the altitude (representing air density), and α is the angle of attack of the vehicle. It is assumed that the sideslip angle β is kept small so that its influence can be neglected.

The data underlying the present representation are taken from Reference 22 for a limit temperature of 1093°C (2000°F). Figure 2a shows a qualitative picture of typical altitude constraints caused by dynamic pressure and kinetic heating. The effects of both velocity and lift coefficient are seen to be appreciable for the heating constraint. The heating constraint is more severe than the dynamic pressure boundary for hypersonic speeds (v > 2.5 to 4.5 km/sec, depending on angle of attack).

In the trajectory optimization program, the control C_{LH} on a boundary arc is required as a function of the state variables altitude and velocity.

The data are given in the form [22]

$$\phi(h, v, \alpha) = 0 \quad . \tag{6}$$

Since the use of the lift coefficient C_L instead of angle of attack α reduces the computational workload to represent the aerodynamic characteristics of the vehicle, the relation $C_L(\alpha, h, v)$ is used to eliminate α. The transformed equation (6) is then represented in the form

$$C_{LH} = B_i H_i + \Delta C_{LH} \quad , \quad i = 1, 5 \tag{7}$$

where

$$\begin{aligned} B_i &= G_{i,j} \hat{h}^{(j-1)} \quad , \quad j = 1, 4 \\ H_1 &= b^2h^2/v \\ H_2 &= bh/v - H_1 \\ H_3 &= 1 - bh/v - H_2 \\ H_4 &= v/(bh) - 2 + bh/v - H_3 \\ H_5 &= v^2/(bh)^2 - 3v/(bh) + 3 - bh/v - H_4 \quad , \end{aligned} \tag{8}$$

and ΔC_{LH} is an adjustment parameter. $G_{i,j}$ is a coefficient matrix as follows:

$$\begin{bmatrix} .110717 & .834519 & 1.213679 & -1.060833 \\ -.672677 & 2.73417 & -.864369 & -12.100000 \\ .812241 & 2.337815 & 10.316280 & 22.974860 \\ -3.151267 & -13.621310 & -40.485500 & -57.833330 \\ 2.368095 & 19.073400 & 69.86905 & 127.777778 \end{bmatrix} \tag{9}$$

and $\hat{h}$ is a coordinate transformed altitude

$$\hat{h} = h/50\ [km] - 1 \tag{10}$$

to keep the coefficients closer to 1. The constant $b = 0.095$ serves the same purpose for the velocity. This form has been obtained by intuition and trial. It is a bivariate polynomial of third order in the altitude and fourth order in velocity. With

$$C_i = \sum_{j=1}^{4} (j - 1)\, G_{i,j}\, \hat{h}^{(j-2)} \quad , \tag{11}$$

the partial derivatives may be written

$$\partial C_{Lh}/\partial v = B_i\, \partial/\partial v\, (H_i) \tag{12}$$

$$\partial C_{Lh}/\partial h = C_i\, H_i + B_i\, \partial/\partial h\, (H_i) \quad . \tag{13}$$

From the form (6), one obtains the partial for constant C_{LH}

$$\partial h/\partial v\Big|_{C_{LH}} = -\frac{\partial C_{LH}}{\partial v} \Big/ \frac{\partial C_{LH}}{\partial h} \quad . \tag{14}$$

The function generated as above is shown in Figure 2b.

The accuracy of the approximation is indicated in Figure 2b by dots representing the original input data into the curve-fit procedure. These points had been obtained from Reference 22 through a crossplot. Except for the 70-km curve, the approximation is good considering the uncertainty in the original data. For maximum range and minimum energy-loss trajectories, which result in lift coefficients in the vicinity of maximum L/D (around $C_L = 0.2$), the 70-km curve will not be needed. Aside from that, the deviation is on the safe side. Below $v = 2.5$ [km/s], the constraint equation is not being used.

Equations of Motion

For the coordinate system, a flight-path-oriented axis system is chosen (Fig. 3). The x-axis is tangential to the trajectory, positive in the flight direction. It is inclined relative to the horizon by the flight-path angle γ, positive upward. The heading

angle χ designates the orientation of the horizontal velocity component relative to the initial time t_o, positive from north over east. The range angle in the original orbit plane is $\oslash$ and Λ (lateral range) is normal to it.

Five controls exist: two associated with the aerodynamic forces and three with the thrust forces. The magnitude of the lift coefficient C_L and the lift bank angle μ, positive from the vertical for increasing heading, determine directly the plane changing force component $C_L \sin \mu$ Fq. The lift coefficient also controls the drag according to equation (4). The three thrust controls are the thrust magnitude, for fixed jet velocity [equation (5)] governed by the mass flow rate $b = \dot{m}/m_o$, the plane-changing thrust angle ϵ, measured from the vertical plane containing the velocity vector, and the thrust angle σ in the vertical plane, measured from the velocity vector. This leads to the following system of equations of motion:

		Inertial	Atmospheric	Propulsive	
$\dot{v}$	=	$-g \sin \gamma$	$-D/m$	$+ \frac{T}{m} \cos \epsilon \cos \sigma$	
$\dot{\chi}$	=	$-\frac{v}{r} \cos \gamma \cos \chi \tan \Lambda$	$+ \frac{L \sin \mu}{mv \cos \gamma}$	$+ \frac{T}{mv} \frac{\sin \epsilon}{\cos \gamma}$	
$\dot{\gamma}$	=	$\left(\frac{v}{r} - \frac{g}{v}\right) \cos \gamma$	$+ \frac{L}{mv} \sin \mu$	$+ \frac{T}{mv} \cos \epsilon \sin \sigma$	
$\dot{\oslash}$	=	$\frac{v}{r} \frac{\cos \gamma}{\cos \Lambda} \cos \chi$			(15)
$\dot{\Lambda}$	=	$\frac{v}{r} \cos \gamma \sin \chi$	Kinematic relations		
$\dot{r}$	=	$\dot{h} = v \sin \gamma$			
$\dot{m}$	=	$-b$			

where

$$\begin{bmatrix} L \\ D \end{bmatrix} = \begin{bmatrix} C_L \\ C_D \end{bmatrix} F \frac{\rho}{2} v^2$$

are the aerodynamic force components, lift and drag.

Boundary Conditions

A complete synergetic plane change maneuver only has the specifications of the initial and final orbit as boundary conditions. By removing the legs of the total maneuver that are outside of the denser atmosphere, as is done here to reduce computational difficulties, somewhat arbitrary boundary conditions are introduced. As will be shown in the discussion of the results, some complications may be encountered because of this procedure.

Using engineering judgement, the range of entry and exit parameters can be narrowed considerably. The "edge" of the denser atmosphere may be defined as the altitude in which the total aerodynamic force grows to a threshold percentage of the gravitational force.

In this study the altitude, h = 80 km , has been selected even though at this level heating is already significant. Velocity losses caused by drag above this level can be estimated analytically [19].

From the qualitative picture of the heating constraint in Figure 2a, it may be seen that minimum altitudes during the skip cannot be expected below 30 km. The entry velocity for a return from a 550 km (300 nm) circular earth orbit is around 7.95 km/s. From these numbers, an estimation of favorable entry flight path angles may be obtained. From energy and angular momentum relations for elliptic vacuum orbits using small angle approximations ($\sin \gamma_e \approx \gamma_e$, $\cos \gamma_e \approx 1 - \gamma_e^2/2$) , one obtains

$$\gamma_e = -\left\{1 - 2\left(\frac{v_{se}}{v_e}\right)^2 \frac{r_p}{r_e} + \left[2\left(\frac{v_{se}}{v_e}\right)^2 - 1\right]\left(\frac{r_p}{r_e}\right)^2\right\}^{1/2} \tag{16}$$

where v_{se} is the satellite velocity in the entry altitude and r_p is the perigee radius. The entry angles for v_e = 7.95 km/s and entry altitude of 80 and 95 km corresponding to perigee altitudes of 30 to 60 km are given in Table 1.

It is seen that for this entry velocity, the flight path angle at 80 km is about 0.25 deg shallower than at 95-km altitude. To just hit the heating constraint with the vacuum perigee altitude at maximum L/D, the entry flight path angle should be around -0.7 to -0.8 deg. This small flight path angle, however, results in a long descent arc, long maneuver time and larger total heat inputs. Therefore, a nominal entry angle of -1.25 deg at 80 km has been chosen. This results in conservative trajectories since both the descent and the ascent propellant requirements are somewhat higher than that required for the maneuver. The effect of entry flight path angle on the atmospheric flight arc will be discussed later.

TABLE 1. ENTRY FLIGHT PATH ANGLES IN DEGREES FOR v_e = 7.95 km/s

h_e/km \ h_p/km	30	40	50	60
95	-1.393	-1.266	-1.13	-0.983
80	-1.151	-1.015	-0.866	-0.697

The exit boundary conditions for the heading angle χ and the lateral range Λ determine the plane change angle i . Combining the inertial term of the second equation with the fifth equation in equation (15) yields

$$\cos \chi^* \cos \Lambda^* = \cos \chi \cos \Lambda \quad . \tag{17}$$

after integration. For $\Lambda^* = 0$, the heading angle χ^* is identical to the plane change angle i . It is assumed that on the upgoing leg beyond the specified boundary values of v_f = 7.95 km/s and h_f = 80 km no further plane change takes place. The relation between plane change angle i , heading angle at exit χ_f , and the lateral range Λ_f in the parameter range of interest here is plotted in Figure 4.

In the numerical iterations, the final heading angle χ_f had been specified, and the lateral range was left free to assume the most favorable value. The full dots in Figure 4 show that the plane change achieved is approximately a fixed percentage ($\approx$ 1.4 percent) higher than the specified heading for the unconstrained trajectories. In the constrained cases (light circles), the percentage increases with specified final heading angle. When comparing both cases, this difference has to be considered.

Resulting from similar considerations with respect to maneuver range and total heat transfer as for the entry, the exit flight path angle has been selected to be γ_f = 1.5 and 2 deg, respectively (see also Fig. 12 of Ref. 20). The specification of γ_f may have a strong influence on the optimal burn time as will be discussed later. Small exit angles may result in a split of the ascent burn phase.

The approach taken results in the following set of boundary conditions for the system of differential equations (15):

Variable	Initial Conditions	Final Conditions
v/km/s	7.95	7.95
$\chi/^\circ$	0	Specified
$\gamma/^\circ$	Specified	Specified
$\Lambda/^\circ$	0	Free
h/km	80(95)	80(95)
m/m_o	1	To be maximal

The downrange angle Θ does not enter the differential equations and was therefore omitted.

REDUCTION TO A BOUNDARY VALUE PROBLEM BY APPLICATION OF THE MAXIMUM PRINCIPLE

The nonlinear optimal control problem with six state and five control variables is reduced to a boundary value problem, which has to be solved numerically, by the application of the maximum principle.

The Hamiltonian function is from equations (1), (5), and (15):

$$H = \frac{v}{r}\cos\gamma\left[\lambda_\gamma\left(1-\frac{gr}{v^2}\right)+\frac{\cos\chi}{\cos\Lambda}\left(\lambda_\Theta-\lambda_\chi\sin\chi\right)+\lambda_\Lambda\sin\chi\right]+\sin\gamma\left(v\lambda_h-g\lambda_v\right)$$

$$+\frac{F\rho_o}{2m}ve^{-\beta h}\left[C_L\left(\lambda_\chi\frac{\sin\mu}{\cos\gamma}+\lambda_\gamma\cos\mu\right)-v\lambda_v C_D\right]$$

$$+b\left\{\frac{U_e}{mv}\left[\left(v\lambda_v\cos\sigma+\lambda_\gamma\sin\sigma\right)\cos\epsilon+\frac{\lambda_\chi}{\cos\gamma}\sin\epsilon\right]-\lambda_m\right\}. \qquad (18)$$

The auxiliary (costate) variables λ are given by the differential equations

$$\dot{\lambda} = -\partial H/\partial X \qquad (19)$$

which are derived in the appendix.

Determination of the Optimal Controls

Since the payoff quantity final mass is to be maximized, the Hamiltonian has to be minimal with respect to all controls

$$U^T = (C_L , \mu , b , \sigma , \epsilon) \quad .$$

Extremal Bank Angle. The expression $\left(\lambda_\chi/\cos \gamma\right) \sin \mu + \lambda_\gamma \cos \mu$ has its minimum $-w_a$ with respect to μ

$$-w_a = -\left[\left(\frac{\lambda_\chi}{\cos \gamma}\right)^2 + \lambda_\gamma^2\right]^{1/2} \tag{20}$$

for

$$\sin \mu^* = \lambda_\chi/(-w_a \cos \gamma) \quad , \quad \cos \mu^* = -\lambda_\gamma/w_a \quad . \tag{21}$$

Extremal Lift Coefficient. The square-bracket expression in the second line of equation (18) contains all lift coefficient terms. Using equation (4) for the drag polar yields $\partial H/\partial C_L = 0$ for

$$C_L{}^* = \left[-w_a/(v\lambda_v \, kn)\right]^{1/(n-1)} \tag{22}$$

Extremal Thrust Magnitude. In the third line of equation (18), the mass flow b appears linearly so that the expression in the outer bracket acts as a switching function

$$S_T = U_e(-w_T)/(mv) - \lambda_m \quad . \tag{23}$$

Depending on the size of S_T , the following values for control b have to be chosen (for w_T see below):

$S_T > 0$	$b = 0$	
$S_T = 0$	Intermediate thrust arc (singular case)	
$S_T < 0$	$b = b_{max}$	(24)

Extremal Thrust Direction in Vertical Plane. The innermost bracket in the third line of equation (18) has its minimum with respect to σ for

$$\sin \sigma^* = -\lambda_\gamma / w_1 \quad ; \quad \cos \sigma^* = -v\lambda_v / w_1 \tag{25}$$

with

$$-w_1 = -\left[(v\lambda_v)^2 + \lambda_\gamma{}^2\right]^{1/2} \quad . \tag{26}$$

Extremal Plane Changing Thrust Angle. With equation (26), the middle bracket in the last row of equation (18) may be written as

$$-w_1 \cos \epsilon + \left(\lambda_\chi / \cos \gamma\right) \sin \epsilon \quad ,$$

which has its minimum with respect to ϵ for

$$\sin \epsilon^* = \lambda_\chi / (-w_T \cos \gamma) \quad ; \quad \cos \epsilon^* = w_1 / w_T \tag{27}$$

with

$$-w_T = -\left[w_1{}^2 + (\lambda_\chi / \cos \gamma)^2\right]^{1/2} \quad . \tag{28}$$

From equations (25) and (27) follows

$$\cos \epsilon^* \cos \sigma^* = -v\lambda_v / w_T$$

and

$$\cos \epsilon^* \sin \sigma^* = -\lambda_\gamma / w_T \quad . \tag{29}$$

Now, the extremal controls are given at each instant as a function of the state and costate variables.

For each unspecified boundary value of the state variables there is a relation given from the transversality conditions for the corresponding boundary values of the costate variables so that in total 2n boundary values specify the solution to the 2n-system of differential equations (15) and (19). The requirement $H_f = 0$ determines the final time.

Constraint Arcs

On constraint arcs involving one control directly, the constraint equation

$$C(\underline{X}, u) = 0 \tag{30}$$

determines the control as a function of the state [23]. For the constraint to remain satisfied, the following relation has to hold

$$\frac{\partial C}{\partial x}\,\delta x + \frac{\partial C}{\partial u}\,\delta u = 0 \quad . \tag{31}$$

This yields

$$\delta u = -\left(\frac{\partial C}{\partial u}\right)^{-1} \frac{\partial C}{\partial \underline{X}}\,\delta X \tag{32}$$

which when introduced into the linearized perturbation equation

$$\delta \dot{X} = \frac{\partial f}{\partial \underline{X}}\,\delta X + \frac{\partial f}{\partial u}\,\delta u \tag{33}$$

leads to

$$\delta \dot{X} = \left[\frac{\partial f}{\partial \underline{X}} - \frac{\partial f}{\partial u}\left(\frac{\partial C}{\partial u}\right)^{-1} \frac{\partial C}{\partial \underline{X}}\right] \delta X \quad . \tag{34}$$

The costate (adjoint) differential equations therefore have additional terms on constraint arcs, where the control is being determined from the constraint equation

$$\dot{\lambda} = -\left[\frac{\partial f}{\partial \underline{X}} - \frac{\partial f}{\partial u}\left(\frac{\partial C}{\partial u}\right)^{-1} \frac{\partial C}{\partial \underline{X}}\right]^T \lambda \quad . \tag{35}$$

For the heating constraint (6) which may be written in the form

$$C = C_L - C_{LH}(h, v) \leqslant 0 \quad , \tag{36}$$

the following terms are obtained:

$$\frac{\partial C}{\partial X} = -\left[\frac{\partial C_{LH}}{\partial v} \quad 0 \quad 0 \quad 0 \quad \frac{\partial C_{LH}}{\partial h} \quad 0\right] \quad , \tag{37}$$

where $X^T = (v, \chi, \gamma, \Lambda, h, m)$,

$$\frac{\partial C}{\partial C_L} = 1 \tag{38}$$

and from equation (15) $[\dot{X} = f(X,u)]$ results

$$\frac{\partial f}{\partial u}\left[\frac{\partial C}{\partial u}\right]^{-1}\frac{\partial C}{\partial X} = -\frac{F\rho}{2m}\, v \begin{bmatrix} -v\dfrac{\partial C_D}{\partial C_L}\dfrac{\partial C_{LH}}{\partial v} & 0 & 0 & 0 & -v\dfrac{\partial C_D}{\partial C_L}\dfrac{\partial C_{LH}}{\partial h} \\ \dfrac{\sin\mu}{\cos\gamma}\dfrac{\partial C_{LH}}{\partial v} & 0 & 0 & 0 & \dfrac{\sin\mu}{\cos\gamma}\dfrac{\partial C_{LH}}{\partial h} \\ \cos\mu\dfrac{\partial C_{LH}}{\partial v} & 0 & 0 & 0 & \cos\mu\dfrac{\partial C_{LH}}{\partial h} \\ 0 & 0 & 0 & 0 & 0 \\ 0 & 0 & 0 & 0 & 0 \\ 0 & 0 & 0 & 0 & 0 \end{bmatrix} . \tag{39}$$

This yields, as additional terms in the costate equations on constraint arcs,

$$\dot{\lambda}_{v_c} = \dot{\lambda}_{v_{uc}} + \frac{\partial C_{LH}}{\partial v} K \tag{40}$$

$$\dot{\lambda}_{hc} = \dot{\lambda}_{h_{uc}} + \frac{\partial C_{LH}}{\partial h} K \tag{41}$$

where

$$K = \left(- w_a + v\lambda_v \frac{\partial C_D}{\partial C_L} \right) \frac{F\rho}{2m} v \tag{42}$$

SOLUTION OF THE BOUNDARY VALUE PROBLEM BY MULTIPLE SHOOTING

The majority of the numerical solutions discussed in the next section were generated by a multiple shooting algorithm [24]. Initial gliding solutions were obtained by a min-H gradient program. Then, by using continuation methods in several parameters, the glide-thrust trajectories were generated with a general multiple shooting subroutine due to Bulirsch [25]. This isolation scheme has convergence properties ranging from those of simple shooting to those of the generalized Newton-Raphson algorithm depending on the number of segments used [25, 26]. It may be viewed as a compromise for combining low storage requirements and easy adaptation to new problems of the simple shooting with the possibility of generating iterates not from just one set of variables at one point in time. By the introduction of intermediate grid points, the sensitivity of variables at one boundary with respect to slight changes of variables at the other boundary may be reduced significantly. Numerical errors propagate only over each segment. Figure 5 shows qualitatively the gain to be expected. Only one variable is displayed. The upper two curves for simple shooting show that the computation of the Jacobian matrix by numerical differentiation is not achieved since the trajectory based on poor guesses for the missing initial conditions blows up, a case easily encountered in reentry. With multiple shooting, the trajectory may be restarted at intermediate points using new guesses. Jacobian matrices are formed for each segment. The resulting iteration scheme, based on reducing all discontinuities at internal grid points to zero, leads to a system of linear algebraic equations which can always be reduced to the dimension of the simple shooting problem. The total Jacobian matrix linking the changes of the boundary values at each end to each other is formed as the product of all segmental Jacobians. Through the intermediate grid points, the path along which the total Jacobian is formed can be much better controlled. The price to pay, however, is that for interior segments the Jacobian matrices required are full square matrices, whereas in simple shooting and, of course, for the first segment in multiple shooting, only rectangular matrices diminished by the known initial conditions are required.

Three to five segments, depending on the length of the maneuver, were selected. In regions where aerodynamic forces are significant, segment lengths of 100 to 150 s seem appropriate. On the descending or ascending leg much larger segments could be handled. Figure 6 shows a typical example of the segmentation and iteration. The initial guesses for the second and third segments were relatively poor resulting in large jumps at the intermediate grid points (Figs. 6a and 6b). They are reduced considerably during the first iteration. After convergence, the curves are smooth and the altitude-velocity phase plot ends

at the same point where it started (h = 95 km, v_e = 7.95 km/s, not shown; for similar plots see Fig. 9b). The time histories (Fig. 6c) show that the intermediate grid points are at the beginning, the middle, and the end of the high dynamic pressure region of the trajectory. For vacuum trajectories simple shooting often is a good iteration scheme as can be inferred from the long, low density descending and ascending portions. Without the intermediate grid points, however, convergence will often not be achieved. In the iteration scheme used, the time was normalized to the range $0 \div 1$. Maneuver time adjustment was derived from the requirement that the Hamiltonian function at the final time has to be zero for open final time. This adjustment shows up as a shift of the grid points in an absolute time scale (Fig. 6c).

DISCUSSION OF RESULTS

Unconstrained Finite Thrust Solutions

Figure 7 shows the altitude time histories and the optimal controls for final heading angles up to 40 deg. In Figure 9, phase plots in comparison to constrained trajectories are given. Figure 7a indicates the increasing penetration depth into the atmosphere with increasing plane change. The main thrusting arcs are on the upgoing legs of the skip, and center around an altitude of 60 to 65 km. For the larger plane change angles, the thrusting arcs extend to the right boundary. For certain parameter combinations, the iteration calls for a coast arc between two thrust arcs on the upgoing leg as indicated by the switching function for χ_f = 35 deg in Figure 7b around 500 s. For slightly smaller heading changes, this coast arc would show up. As will be seen later, this upward bending of the switching function seems to be induced by the specification of too small a final flight path angle. From the thrust angle σ in the vertical plane (Fig. 7c), it may be concluded that the upward accelerating component of the first thrust arc helps to reduce drag losses by steepening the flight path angle while the second (short one) at the end with a downward accelerating component (Fig. 7c) helps satisfy the specified end conditions. A similar behavior occurs for χ_f = 12.5 deg and γ_f = 1.5 deg. In these cases, the convergence behavior is very poor. Increasing γ_f to 2 deg at χ_f = 12.5 deg moves the occurence of the second burn arc to higher final heading angles.

From Figure 7b, it is seen that for small plane change angles ($\chi_f \lesssim 7.5$ deg) an initial burn phase appears for the entry angle γ_e = -1.25 deg chosen. It both decreases the flight path angle and reduces the wingloading. The effect on the flight path angle is two-fold: a direct influence caused by the upward thrust component (see circles at t = 0 in Fig. 7c) and an increased centrifugal force caused by the velocity increase. For smaller entry flight path angles, this thrust phase vanishes. With increasing plane change, which leads to increasingly steeper optimal entry flight path angles [20, Fig. 7] in the unconstrained case, the initial value of the switching function for the fixed entry flight path angle considered here increases, indicating that initial burn arcs become less favorable (Fig. 7b).

The plane changing thrust angle ϵ in the upper part of Figure 7c varies around 23 deg with its highest value at the beginning of the thrust phase when the velocity vector to be turned is smallest and decreasing with increasing time and velocity. This optimal thrust angle is well approximated by the analytical solution of References 19 and 20 or the even simpler result $\epsilon^* \approx \tan^{-1}$ (D/L) which yields for L/D = 2.22 used here a value of $\epsilon^* = 24.25$ deg.

The optimal aerodynamic controls are shown in Figures 7d and 7e. The bank angle time histories are similar to those for gliding flight with maximum exit velocity at a given heading and flight path angle [19,20]. The lift coefficient time histories have characteristic kinks at thrust onset and cutoff. During thrust periods they decrease monotonically. The lift coefficient is always in the vicinity of the value for maximum L/D.

Synergetic Plane Change with Heating Constraint

Figure 8 shows results for the nominal parameter set chosen: entry and exit altitude = 80 km, velocity = 7.95 km/s ($v_{se} = 1.01$), entry flight path angle $\gamma_e = -1.25$ deg, initial wing loading $m_o/F = 275$ (kg/m^2), initial thrust acceleration about 1 g_o. Comparing Figure 8a to Figure 7a, it is seen that the minimum altitude decreases much slower with increasing plane change because of the heating constraint. For $\chi_f = 17$ deg, the minimum altitude is 60.45 km compared to 52.7 km in the unconstrained case. The maximum dynamic pressure is reduced to about 6700 N/m^2 (one third of the unconstrained maximum) and the maneuver time is increased by about 65 percent. The maximum normal acceleration is approximately 0.43 g_o compared to about 1.6 g_o in the case with no heating constraint.

A short initial burn arc appears up to higher plane change angles than in the unconstrained cases; for the entry parameters chosen, it vanishes for $\chi_f \gtrsim 13$ deg (Fig. 8b), where the thrust switching function becomes negative initially. If a steeper entry flight path angle would be chosen, the initial burn phase would increase in time and show up for larger plane change angles. The general shape of the thrust switching function is as follows: It starts with a negative slope, passes through a minimum and a maximum and may have a second minimum (not shown), depending on the specified final flight path angle γ_f. This may occur when γ_f is smaller than the selected value of 2 deg. From Figure 8b it is seen that the slope of the switching function at zero crossing between the first minimum and the maximum, i.e., at the beginning of the ascending leg of the trajectory, becomes smaller for increasing plane change angles. If the slope becomes zero at the zero crossing of S_T a singular thrust arc is encountered. This seems to be the case for χ_f somewhat larger than 19 deg for the parameters chosen. Numerical difficulties are encountered which have to be dealt with in a special approach using higher order optimality conditions. This is beyond the scope of the present investigation.

The significant changes between the unconstrained and the heating constrained optimal synergetic maneuver are exhibited in the phase plots of Figure 9: While in the unconstrained case the heading angle varies almost linearly with the flight path angle over the central portion of the trajectory, in the constrained case the flight path angle is almost zero (Fig. 9a) there. The velocity is decreased and after thrust ignition increased again at almost constant altitude; this altitude is almost independent of the inclination change requested and is given grossly by the heating constraint for a lift coefficient correspondi ng to maximum L/D. In the unconstrained case the minimum altitude decreases with increasing plane change angle (Fig. 9b) and thrust is switched on at positive flight path angles.

The optimal control time histories for the heating constrained skips are shown in Figures 8c through e for final heading angles of 7.5 to 19 deg. The plane changing thrust angle ϵ is seen to be in the vicinity of $\tan^{-1}$ (D/L) = 24.3 deg for L/D = 2.22 as has been estimated by the analytical approximate impulsive solution of References 19 and 20. There is an upward thrust component in the vertical plane (σ around 10 to 15 deg in Figure 8c) the average of which decreases with increasing plane change angle as has been indicated from the impulsive approximation [19,20]. The aerodynamic bank angle μ (Fig. 8d) is in the region of 60 to 85 deg for portions of the trajectory with relatively high dynamic pressure. The small initial values are due to the steeper entry angle chosen here as will be discussed later with reference to Figure 12b. The lift coefficient (Fig. 8e) varies around the value for $(L/D)_{max}$ with characteristic jumps in the slope as the heating constrained arc is entered or left. The high values of C_L at the end occur when the vehicle has already left the denser atmosphere. The last corner in $C_L(t)$ is due to the end of the burn phase. In Figure 10 the mass ratio left after a plane change angle i is given for a complete maneuver to turn a 556 km (300 n.mi.) circular orbit. The exit velocity of the rocket engines on which the figure is based is 4.36 km/s. It is seen that the losses caused by the heating constraint are relatively small. The synergetic plane change maneuver is superior to an extra-atmospheric one for plane change angles i larger than 5 deg. For i = 20 deg the mass ratio in the new orbit is about 15 percent higher after the heating constrained synergetic maneuver, which corresponds to a propellant reduction of about one-third for a shuttle-orbiter type vehicle compared to the extra-atmospheric, one-impulsive plane change.

Sensitivity to Parameter Changes

The most important aerodynamic vehicle parameters are the wing loading m_o/F at the beginning of the skip, the maximum L/D and the heating constraint. Another important parameter for the skip is the entry flight path angle γ_o. Their influence will be discussed for the reference skip trajectory given in Table 2.

An increase in wing loading increases the ratio of inertial to aerodynamic forces for the same state and control of the vehicle. To decelerate the vertical velocity component to zero at the same altitude given by the heating constraint, the bank angle is reduced initially. At the same time, the switching function for the thrust is increased,

TABLE 2. REFERENCE SKIP TRAJECTORY PARAMETERS FOR THE SENSITIVITY ANALYSIS

Wing Loading	$m_o/F = 275$ kg/m^2
Drag Polar Coefficients	$C_{Do} = 04$; $k = 1$; $n = 1.86$ yielding $(L/D)_{max} = 2.22$
Heating Constraint Parameter	$\Delta C_{LH} = 0$, corresponding to $T = 1093°C$ (2200°F)
Jet Velocity	$U_e = 4.36$ km/s
Mass Flow Rate	$\dot{m}/m_o = 2 \cdot 10^{-3}$ [s^{-1}]

	Initial	Final	Initial Adjoint Variable	Final (Costate)
Velocity, km/s	7.95[a]	7.95[a]	-0.1656	-0.1610
Heading Angle, deg	0[a]	15[a]	-0.516	-0.636
Flight Path Angle, deg	-1.25[a]	2.0[a]	-0.289	-0.266
Lateral Range, deg	0[a]	3.83	0.374	0[a]
Altitude, km	80[a]	80[a]	-0.0002453	-0.0003278
Mass Ratio	1[a]	0.8/23[a]	-0.7939	-1[a]

a. Value is preset boundary conditions.

leading to prolonged initial burn times for steep entry angles, thereby supporting the downward deceleration with a positive thrust angle σ and reducing the wing loading for the aerodynamic flight phase. The total propulsion requirement increases slightly more than linearly with m_o, about one third of a percent drop in the final mass ratio for an increase in wing loading from 275 to 300 kg/m^2.

The analytical approximate solutions for the unconstrained skip indicate that the ΔV requirement depends on the maximum lift to drag ratio by the factor exp(-D/L). A numerical test computation validates this dependency also for the heating constrained case.

The effect of changing the severeness of the heating constraint is shown in Figure 11. The adjustment parameter ΔC_{LH} in equation (7) corresponds roughly to a limit temperature change. Letting $\Delta C_{LH} = 0.03$ is an approximation to increasing the limit temperature from 1039°C (2000°F) to about 1204°C (2200°F) for the given data. It shows how a limit temperature increase would affect the trajectory (Fig. 11a) and the controls (Figs. 11b and 11c). The final mass fractions for the three-dimensional atmospheric/thrusting maneuver are

ΔC_{LH}	0	0.03	0.06	Unconstrained
m_f/m_o	0.8123	0.8145	0.8162	0.8200

Due to the heating constraint with $\Delta C_{LH} = 0$, the minimum altitude is lifted from 54 to about 61 km and the maneuver time increases from about 350 to 526 sec (50 percent). The thrust switching function at $t = 0$ decreases for increasing ΔC_{LH}, indicating that initial burn arcs become less favorable for hotter skips. At the same time, the initial bank angle increases (Fig. 11b). From $\mu \approx 90$ deg in the unconstrained case, it is seen $[\mu_{opt} = \tan^{-1}(\lambda\chi/\lambda\gamma \cos\gamma)]$ that the entry flight path angle $\gamma_e = -1.25$ deg is optimal for this parameter set since $\lambda\gamma_o \approx 0$. The lift coefficient time histories again show the characteristic dips on the constrained arcs (Fig. 11c).

The effect of changing the entry flight path angle is shown in Figure 12. The initial short burn phase appears only for entry angles steeper than approximately -1.28 deg. As the entry angle becomes smaller, the ingoing leg of the maneuver changes while the outgoing leg remains essentially unchanged but is shifted in time. In the first half of the trajectory the bank angle increases to about 90 deg using almost all of the lift for plane changing. The maximum final mass fraction is obtained for $\gamma_e \approx -0.78$ deg and is about 0.12 percent higher than for $\gamma_e = -1.25$ deg. This result is obtained without considering viscous interaction effects. With these effects taken into account a steeper entry angle is advantageous [19, 20]. By considering the total heat transfer and the total maneuver time, an entry angle of -1 to -1.25 deg seems to be a good compromise.

CONCLUSIONS

The numerical investigation of the synergetic plane change maneuver for a Space Shuttle orbiter-type vehicle under realistic constraints shows that, for the plane change of a 556-km (300-n.mi.) circular orbit over more than 5 deg, the synergetic maneuver requires less propulsion than an extra-atmospheric one. The kinetic heating constraint results in a markedly different trajectory shaping with much lower maximum dynamic pressure (one-third of the unconstrained case for $\chi_f = 17$ deg) and normal acceleration (only 0.43 g_o compared to 1.6 unconstrained), but only a small decrease in the final mass fraction.

The distribution of the burn arcs is very much dependent on the entry and exit flight path angles given as boundary values. For the nominal values chosen from total range and heat input considerations, an initial burn arc at entry may occur which decreases the flight path angle and reduces the wing loading for the aerodynamic maneuver. If the exit flight path angle is specified too low, the ascent burn phase may have two arcs, one when leaving the denser atmosphere (with an upward accelerating component) and a short second one at the right boundary. The change of the switching function for the thrust when approaching a critical constraint plane change angle, depending on boundary values and vehicle parameters, indicates that a singular thrust arc may be encountered. This question has to be examined in more detail.

The results obtained for a nonrotating earth will be a good approximation for meridional entry in higher latitudes. For plane changes of 20 deg, a saving of 15 percent of the initial mass in propellant corresponding to a one-third propellant reduction may be achieved with the synergetic maneuver as compared to an extra-atmospheric one.

It should be noted that the analysis in this document assumes classical point mass vehicle behavior. The effect of thrust and aerodynamic moments about the vehicle's center of gravity should be examined in future studies to determine if it has any significant effect on the trajectory.

George C. Marshall Space Flight Center
National Aeronautics and Space Administration
Marshall Space Flight Center, Alabama 35812, March 1973.

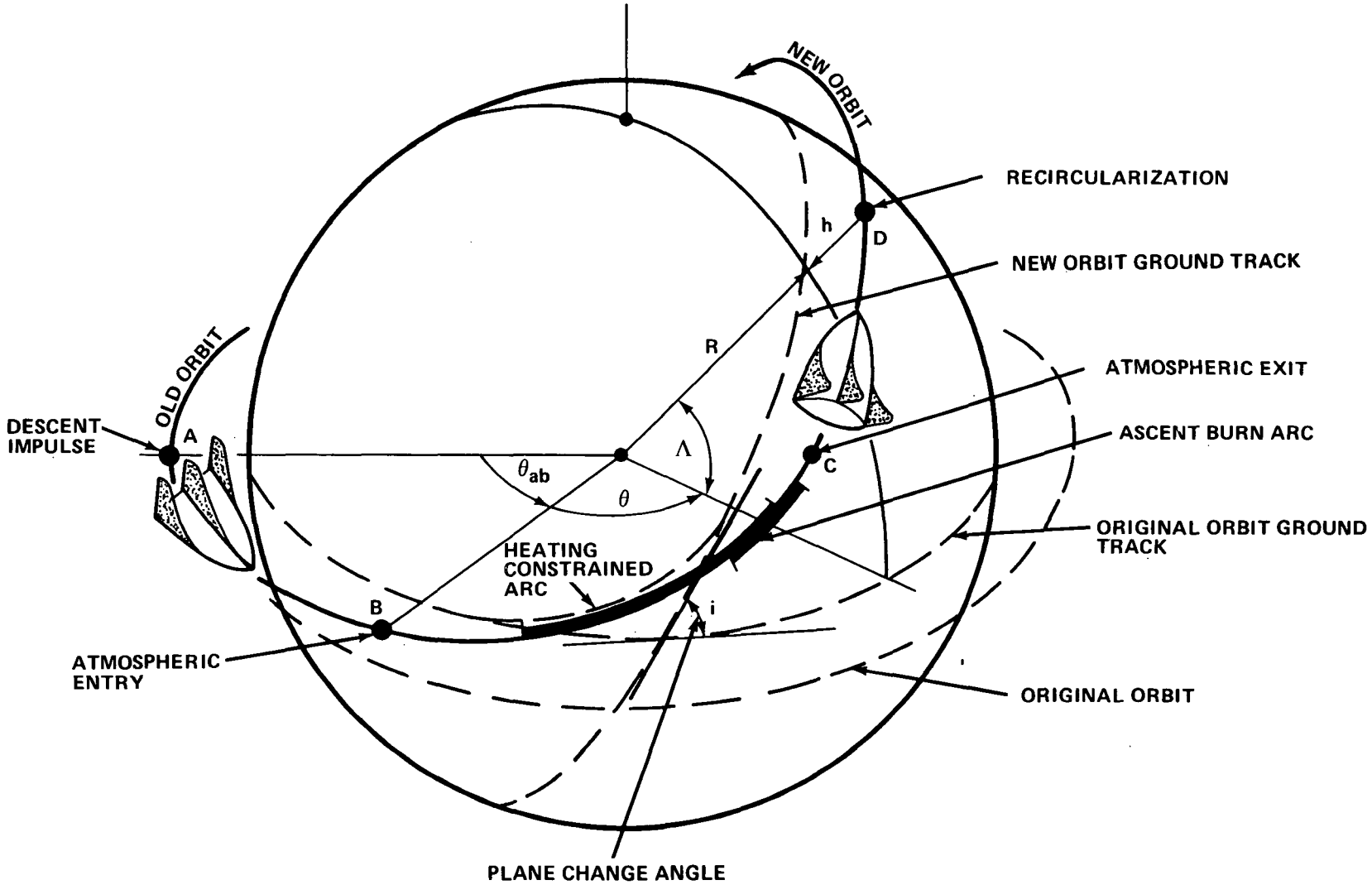

Figure 1. Synergetic plane change maneuver.

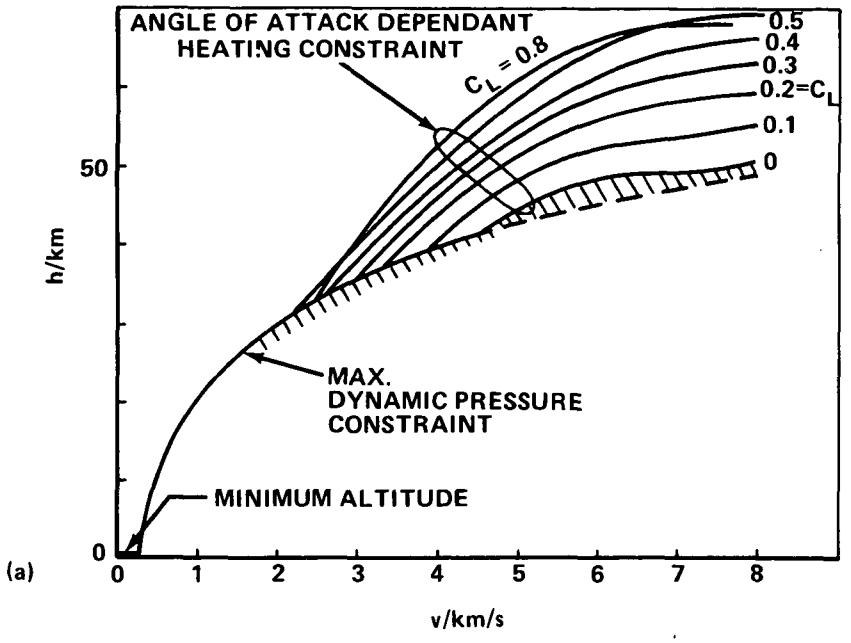

QUALITATIVE ALTITUDE CONSTRAINT FOR REENTRY

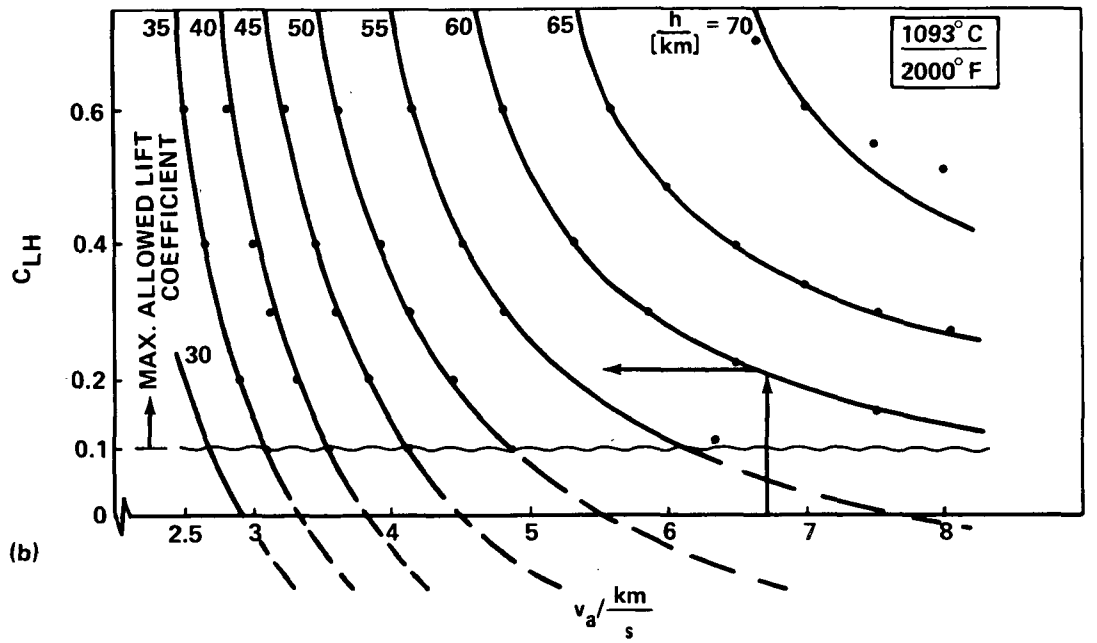

BIVARIATE HEATING CONSTRAINT APPROXIMATIONS

Figure 2. Kinetic heating constraint for Space Shuttle orbiter-type vehicle.

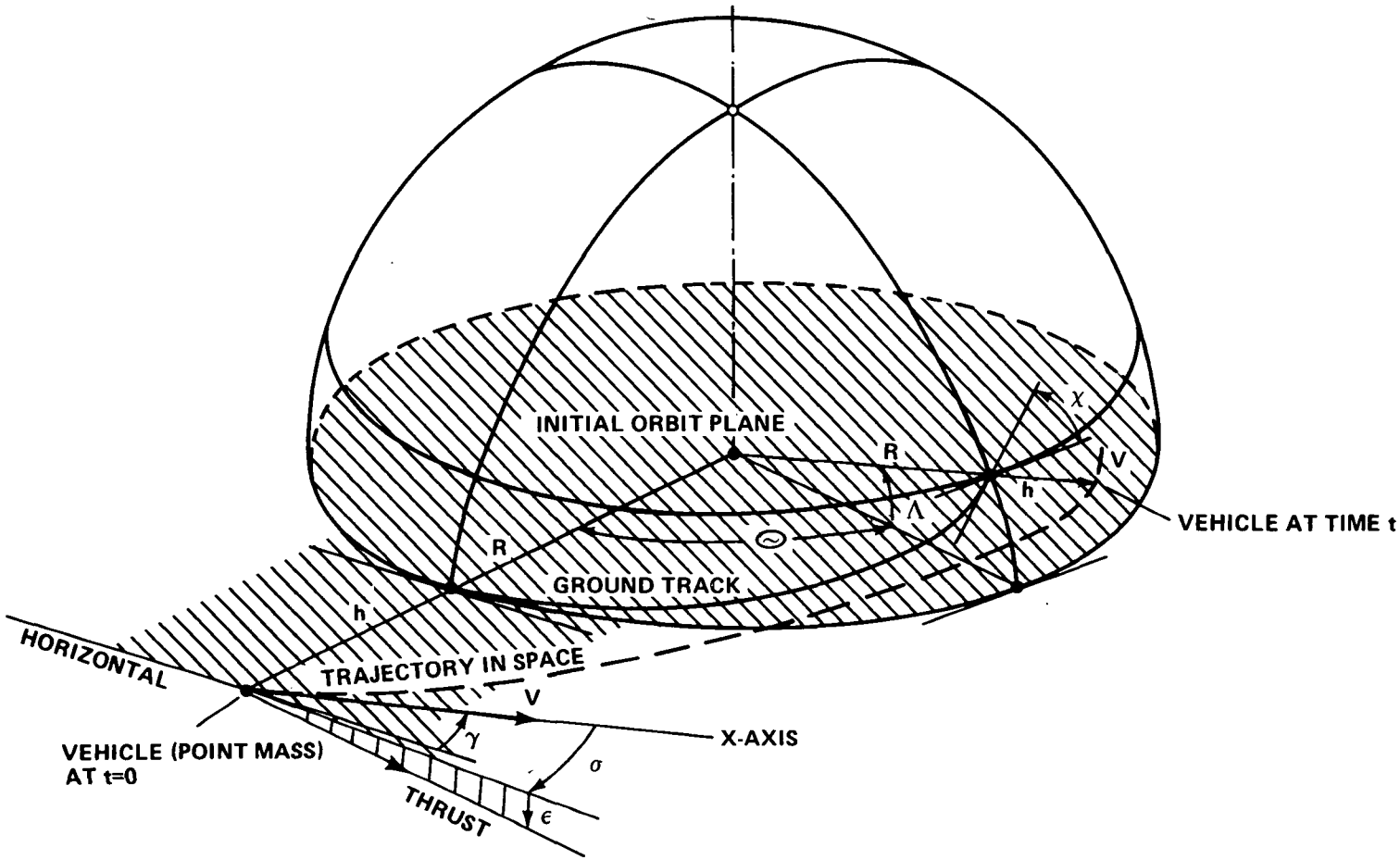

Figure 3. Coordinate system.

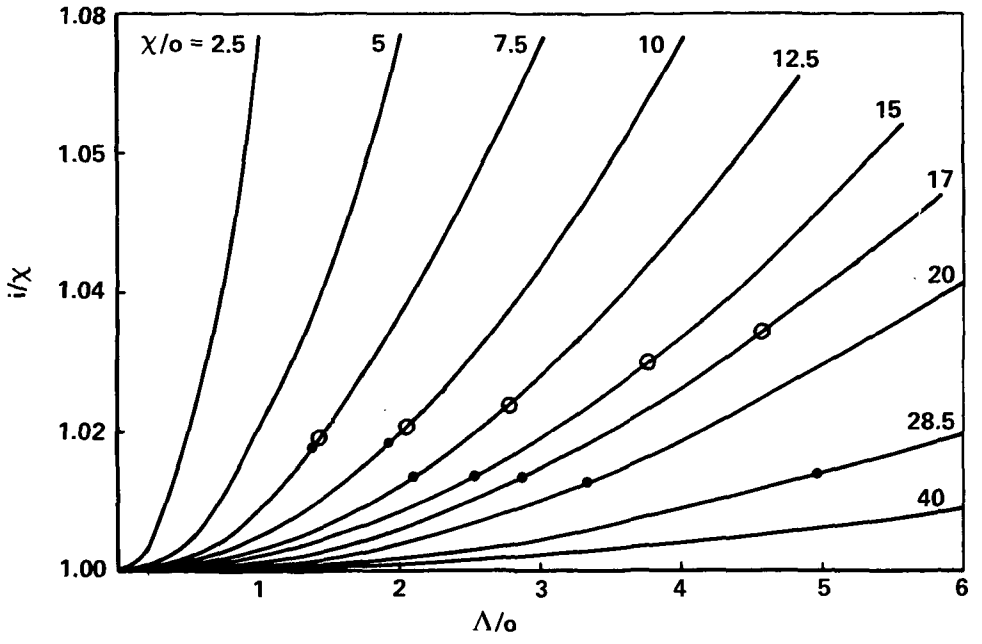

Figure 4. Relation between plane change angle i and heading angle χ_f and lateral range Λ_f for small values of Λ_f.

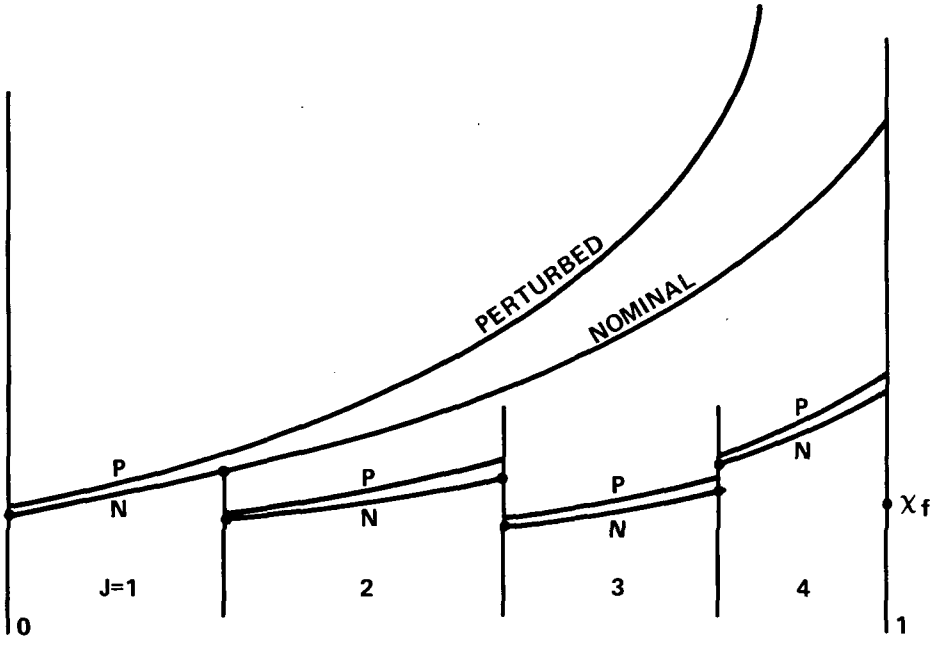

Figure 5. Basic idea of multiple shooting.

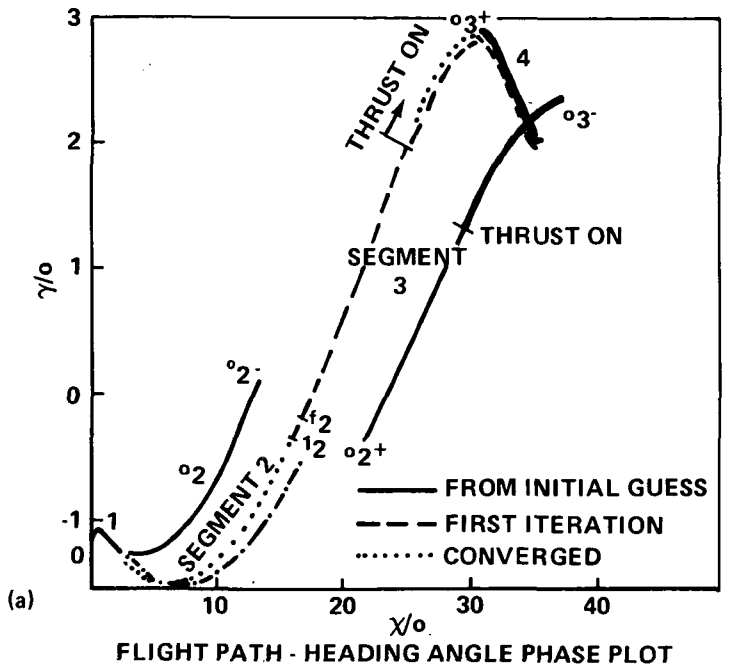

FLIGHT PATH - HEADING ANGLE PHASE PLOT

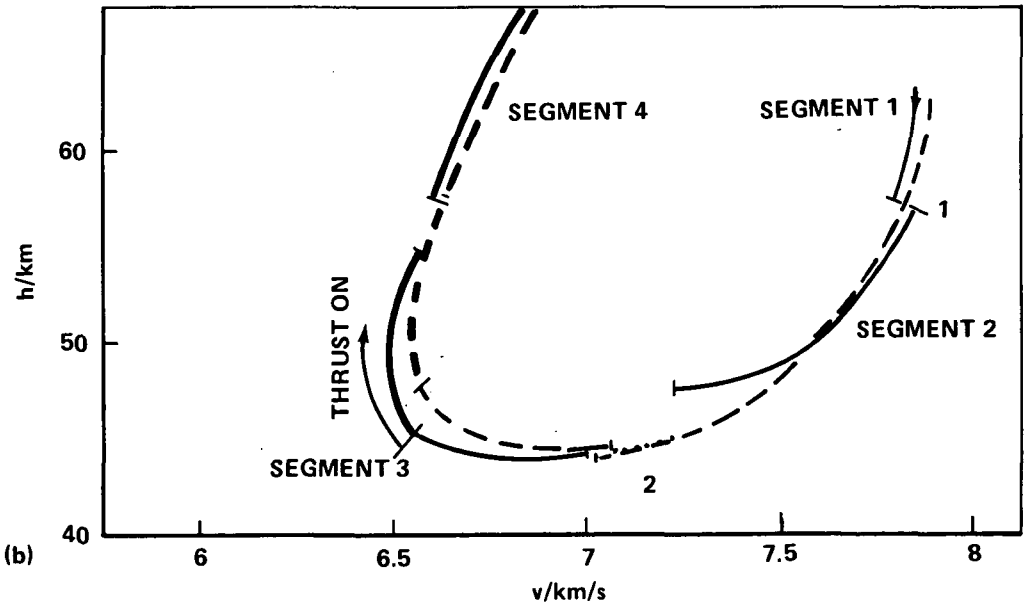

ALTITUDE VELOCITY PHASE PLOT

Figure 6. Multiple shooting optimization of the synergetic plane change. L/D = 2.22, χ_f = 35 deg, U_e = 4.36 km/s, $a_o \approx 1\ g_o$, $v_e = v_f$ = 7.95 km/s, γ_e = -1.25 deg, γ_f = 2 deg, and $h_e = h_f$ = 95 km.

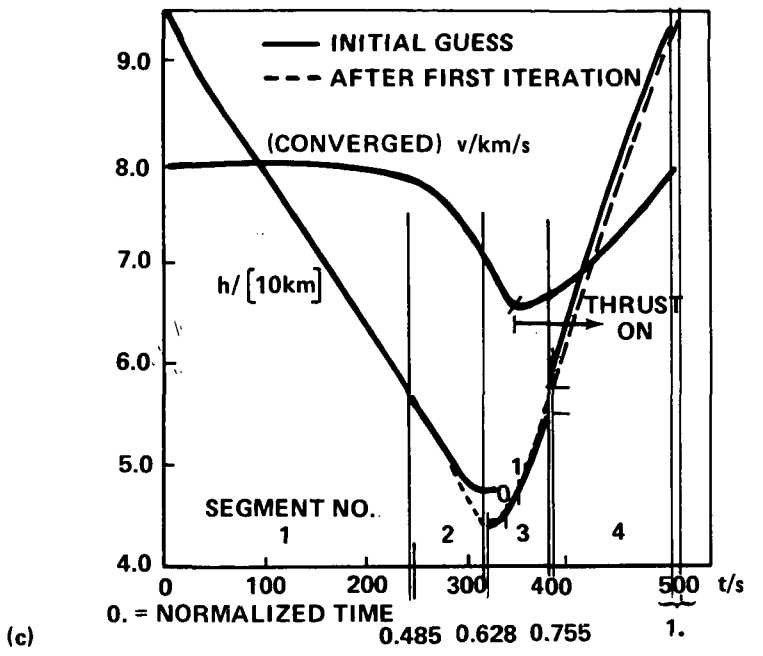

Figure 6. (Concluded).

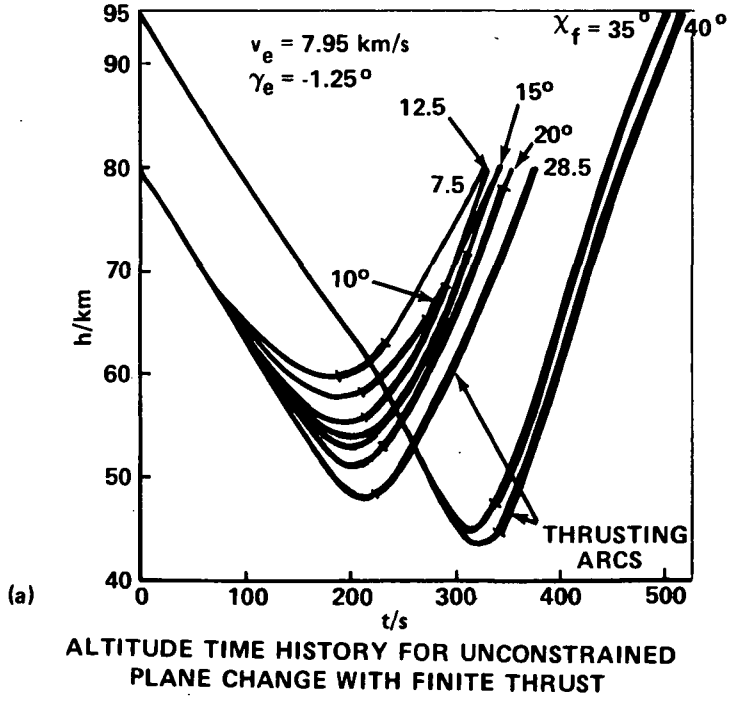

Figure 7. Unconstrained synergetic plane change with finite thrust ($a_{To} \approx 1$ g), $v_e = v_f = 7.95$ km/s, $\gamma_e = -1.25$ deg, and $m_o/F = 275$ kg/m^2.

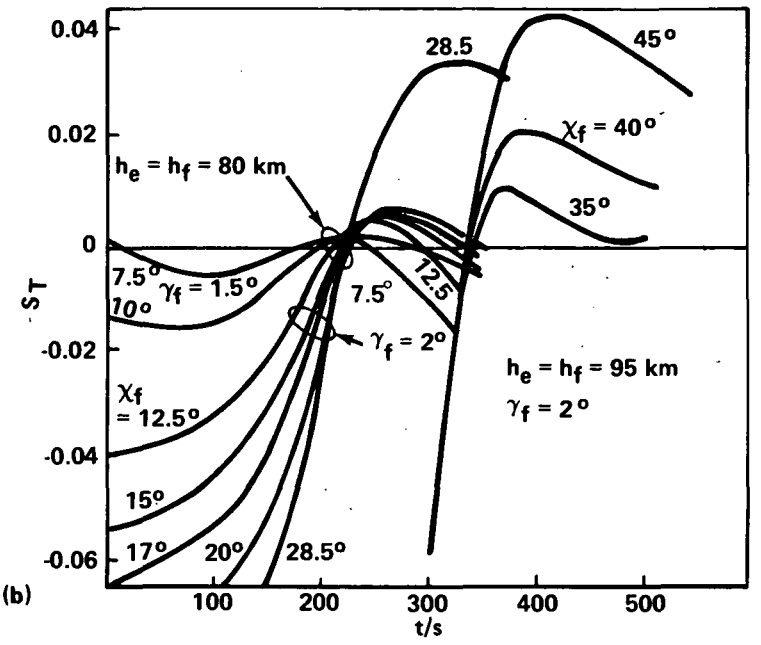

THRUST SWITCHING FUNCTION TIME HISTORIES

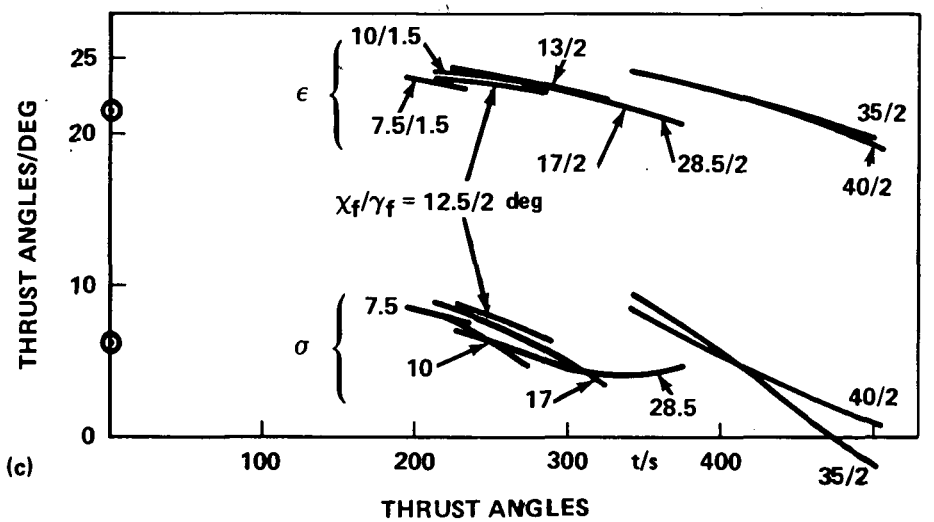

THRUST ANGLES

Figure 7. (Continued).

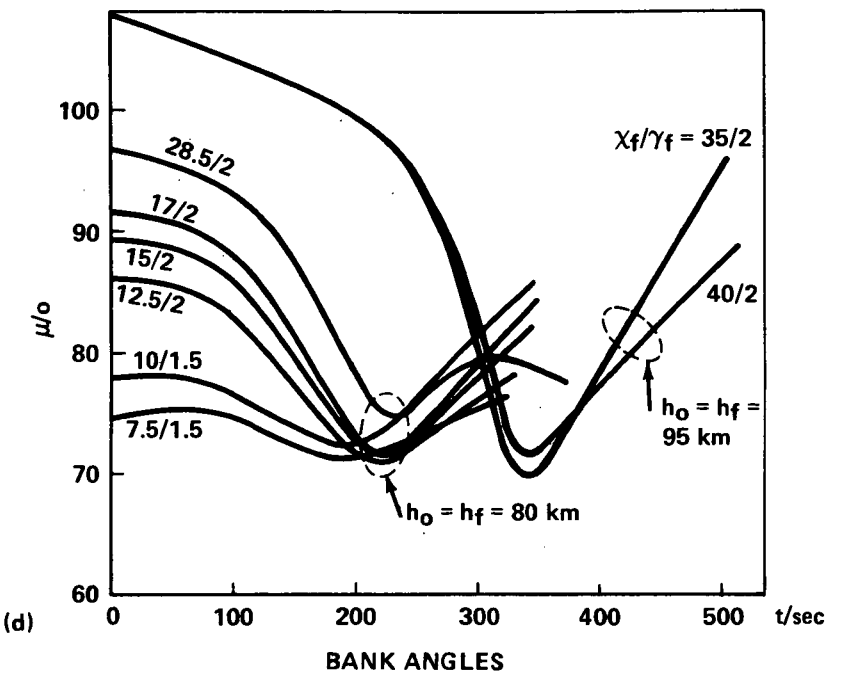

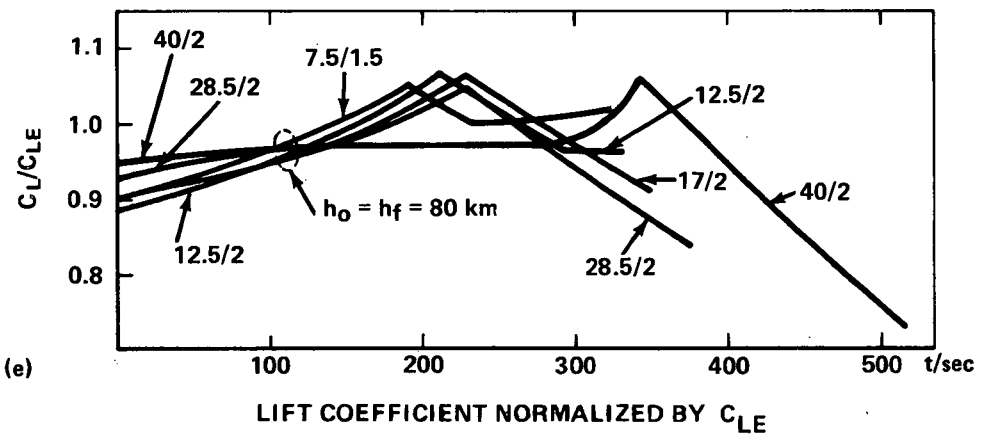

Figure 7. (Concluded).

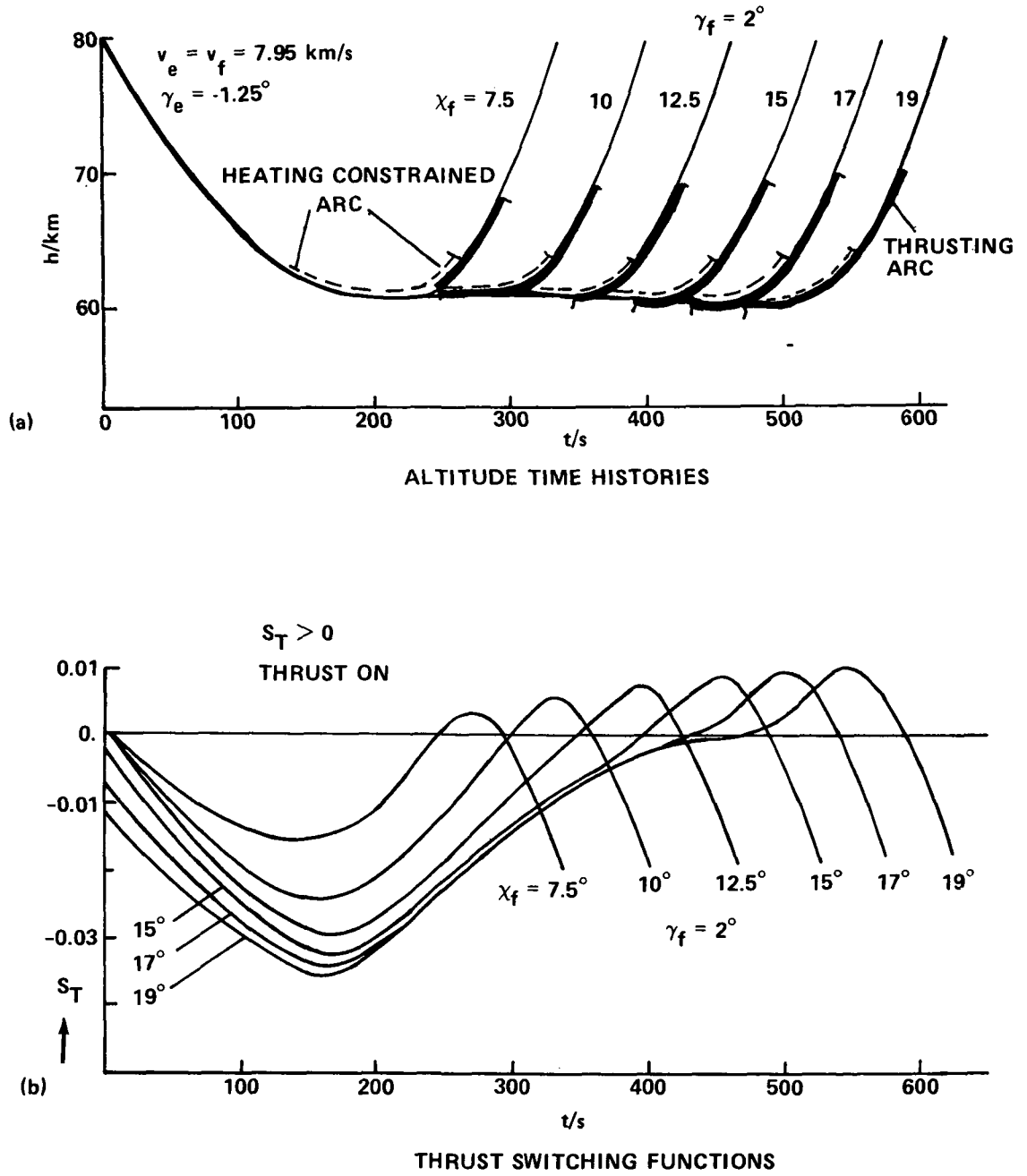

Figure 8. Heating constrained finite thrust synergetic plane change. $v_e = v_f = 7.95$ km/s, $\gamma_e = -1.25$ deg, $h_e = h_f = 80$ km, $m_o/F = 275$ kg/m^2, and $a_{To} \approx 1$ g.

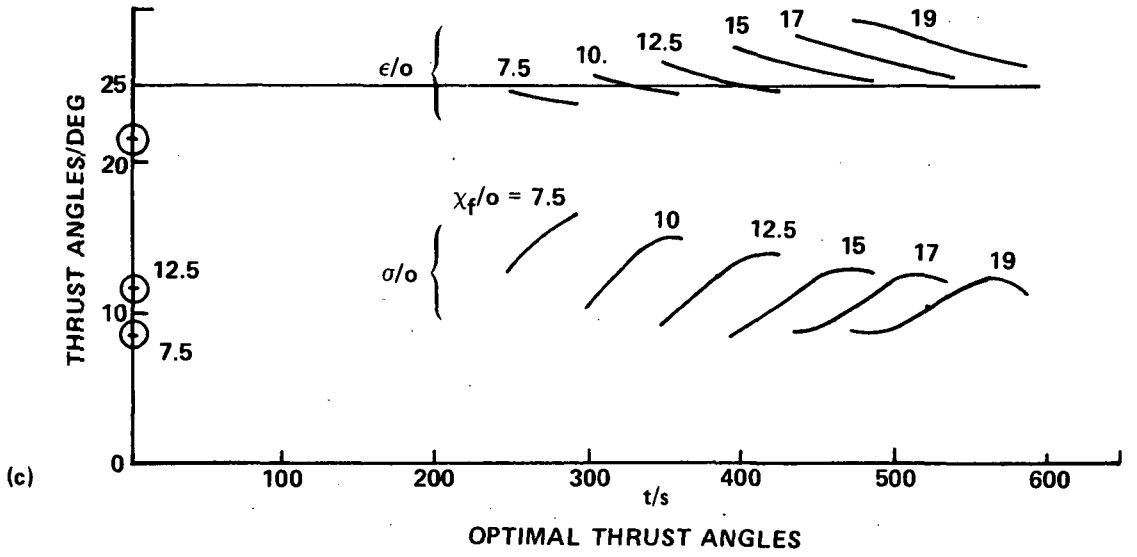

OPTIMAL THRUST ANGLES

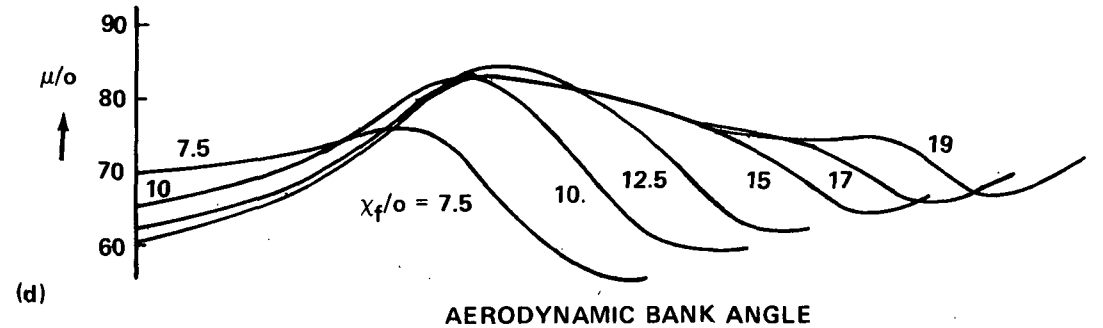

AERODYNAMIC BANK ANGLE

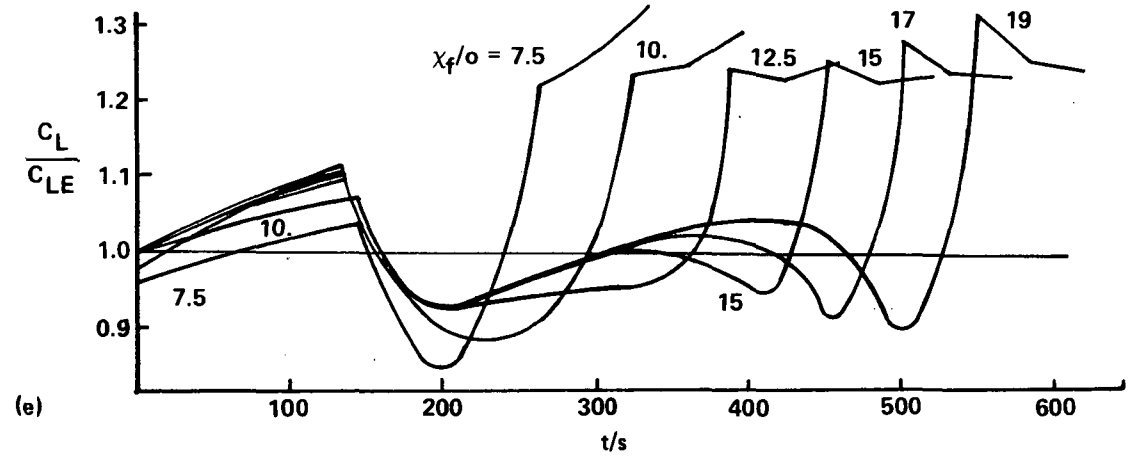

LIFT COEFFICIENT NORMALIZED BY C_{LE}

Figure 8. (Concluded).

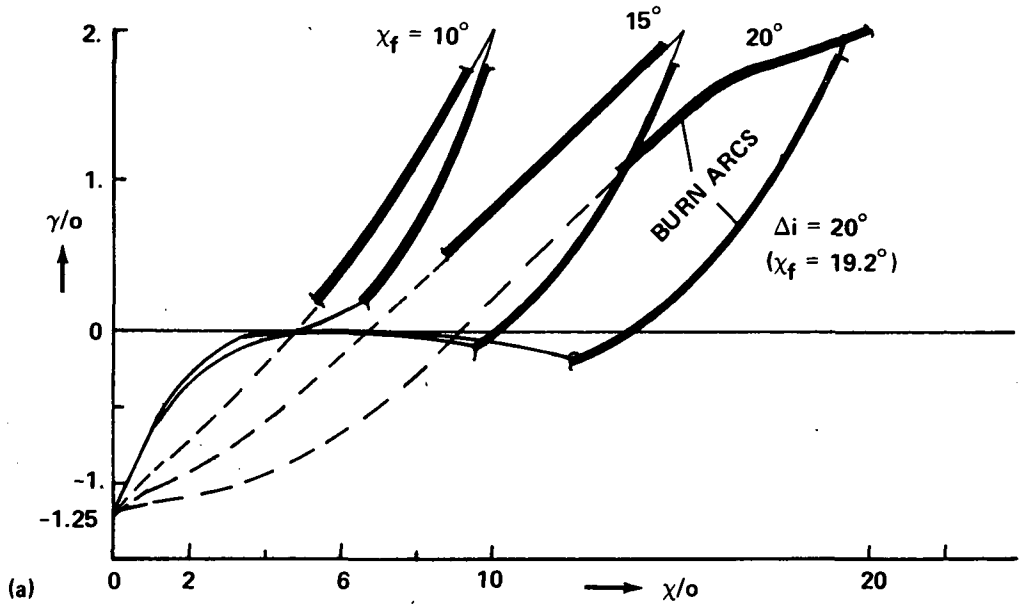

FLIGHT PATH ANGLE VERSUS HEADING

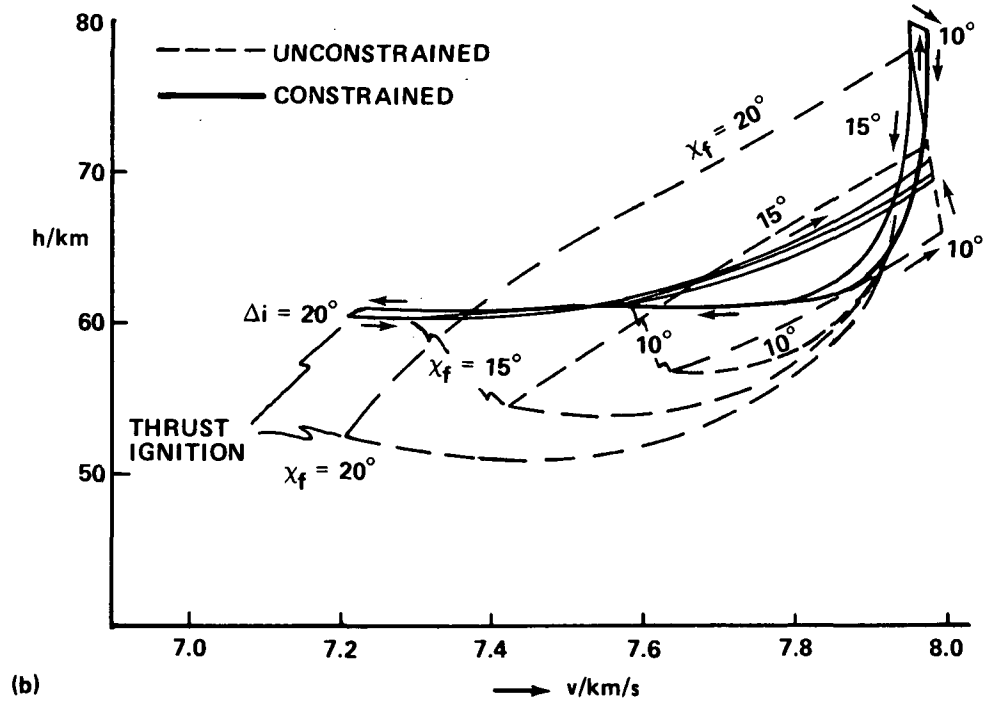

ALTITUDE VERSUS VELOCITY

Figure 9. Phase plots comparing constrained and unconstrained trajectories. m/F = 275 [kg/m^2] and $a_{To} \approx 1$ g.

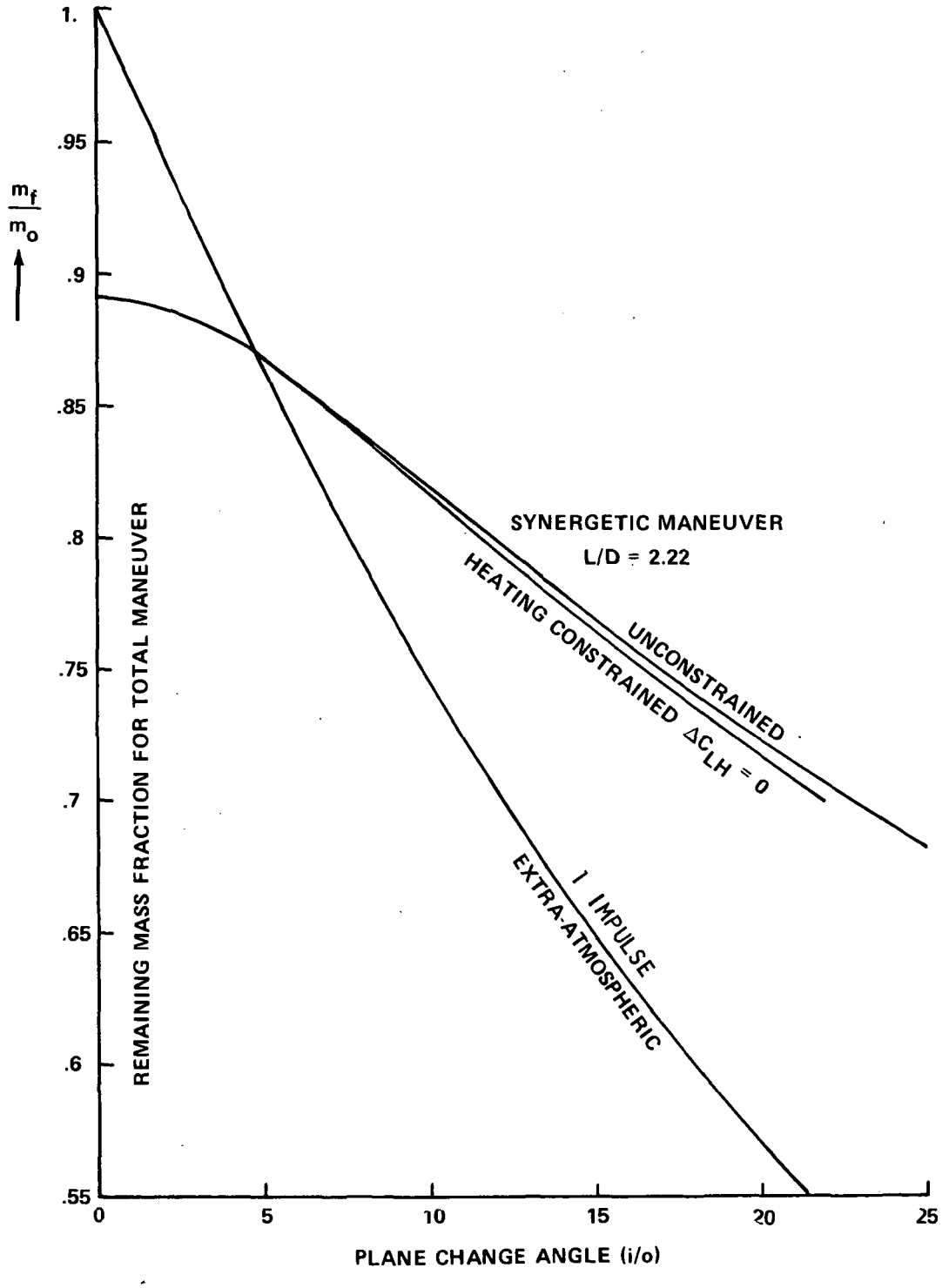

Figure 10. Remaining mass ratio for plane change of a circular 556-km orbit. $U_e = 4.36$ [km/s], $m_o/F = 275$ [kg/m^2], L/D = 2.22, and $\gamma_o = -1.25°$; $\gamma_f = 2°$; $a_T \approx 1\ g_o$.

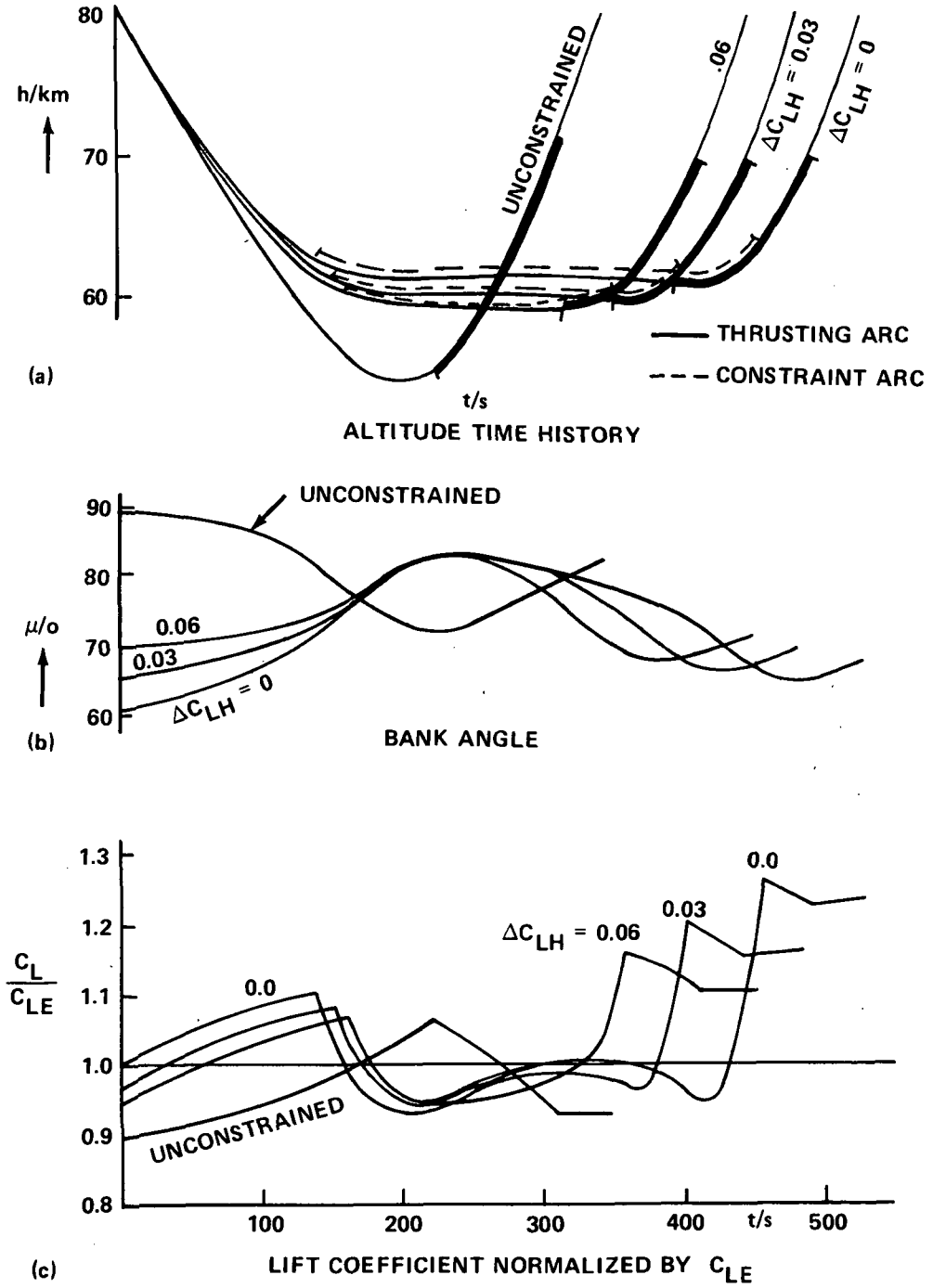

Figure 11. Effect of heating constraint changes on trajectory and controls – $\chi_f = 15$ deg, $\gamma_e = -1.25$ deg, $\gamma_f = 2$ deg, $V_e = V_f = 7.95$ km/s, m/F = 275 [kg/m^2], and $a_{To} \approx 1\ g_o$ ($\Delta C_{LH} = 0.03 \triangleq 200°$ F).

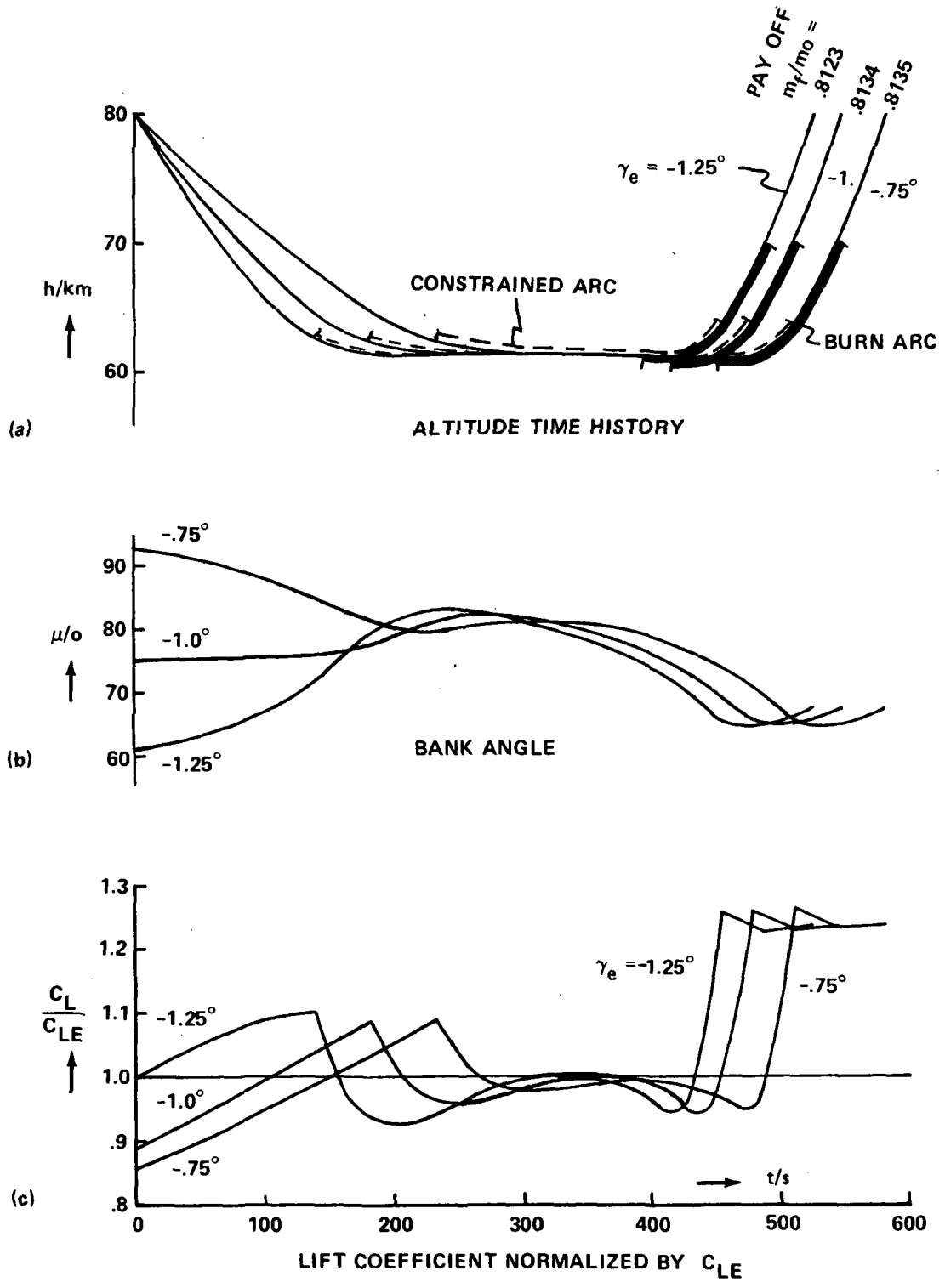

Figure 12. Variation of entry flight path angle – $V_e = V_f = 7.95$ km/s; $\chi_f = 15$ deg, $\gamma_f = 2$ deg, and $m_o/F = 275$ [kg/m^2], $a_{To} \approx 1\ g_o$.

APPENDIX. COSTATE DIFFERENTIAL EQUATIONS

From equations (18) and (19) follows for the differential equations for the Lagrangian multipliers (costate variables):

$$\dot{\lambda}_v = \frac{\cos\gamma}{r}\left[\cos\chi\,\lambda_\chi \tan\Lambda - \lambda_\gamma\left(1+\frac{\Gamma}{v^2 r}\right) - \lambda_\Lambda \sin\chi\right] - \lambda_h \sin\gamma$$

$$+\frac{F\rho_o}{2m}\,e^{-\beta h}\left(2V\lambda_v C_D + C_L w_a\right)$$

$$\dot{\lambda}_\chi = \frac{-v\cos\gamma}{r}\left(\lambda_\chi \sin\chi \tan\Lambda + \lambda_\Lambda \cos\chi\right)$$

$$\dot{\lambda}_\gamma = \cos\gamma\left(\lambda_v\rho - \lambda_h v\right) + \frac{v}{r}\sin\gamma\left[\lambda_\gamma\left(1-\frac{\Gamma}{v^2 r}\right) + \lambda_\Lambda \sin\chi - \lambda_\chi \cos\chi \tan\Lambda\right]$$

$$-\frac{\lambda_\chi}{\cos\gamma}\tan\gamma\,\frac{F\rho_o}{2m}\,e^{-\beta h}\,C_L\,V\sin\mu$$

$$\dot{\lambda}_\Lambda = \frac{v}{r}\,\frac{\cos\gamma\cos\chi}{\cos^2\Lambda}\,\lambda_\chi$$

$$\dot{\lambda}_h = \frac{-2\Gamma}{r^3}\left(\lambda_v \sin\gamma + \frac{\lambda_\gamma}{v}\cos\gamma\right) + \frac{v}{r^2}\cos\gamma\left(\lambda_\gamma + \lambda_\Lambda \sin\chi - \lambda_\chi \cos\chi \tan\Lambda\right)$$

$$-\beta\,\frac{F\rho_o}{2m}\,e^{-\beta h}\,v\left(v\lambda_v C_D + C_L w_a\right)$$

$$\dot{\lambda}_m = -\frac{F\rho_o}{2m^2}\,e^{-\beta h}\,v\left[v\lambda_v C_D + C_L w_a\right]$$

On thrusting arcs, the following terms have to be added:

$$\dot{\lambda}_{vT} = \dot{\lambda}_v - \frac{T}{mv^2}\left[\left(\frac{\lambda_\chi}{\cos\gamma}\right)^2 + \lambda_\gamma^2\right] \Big/ w_T$$

$$\dot{\lambda}_{\gamma T} = \dot{\lambda}_{\gamma} + \frac{T}{mv} \frac{\lambda_{\gamma}^2 \sin \gamma}{\cos^3 \gamma \, w_T}$$

$$\dot{\lambda}_{mT} = \dot{\lambda}_{m} - \frac{T}{m^2 v} \left[\left(v\lambda_v \right)^2 + \left(\frac{\lambda_\chi}{\cos \gamma} \right)^2 + \lambda_\gamma^2 \right]$$

Additive terms for the heating constrained arcs were given as equations (40), (41), and (42).

REFERENCES

1. London, H.S.: Change of Satellite Orbit Plane by Aerodynamic Maneuvering. J. Aero-Sci., vol. 29, pp. 323-332, March 1962.

2. Nyland, F.S.: The Synergetic Plane Change for Orbiting Spacecraft. RM-3231-PR, The Rand Corp., August 1962.

3. Kalil, F.: In Orbit Cross-Range Maneuvers. Martin Co., ER 12929, March 1963.

4. Bell, R.N. and Hankey, W.L.: Application of Aerodynamic Lift in Accomplishing Orbital Plane Change. ASD-TDR-63-693, September 1963.

5. London, H.S.: Comments on Aerodynamic Plane Change. AIAA Journal, vol. 1, no. 10, pp. 2414-2415, October 1963.

6. Nakayama, H.: Comparison of Impulsive Propulsion Requirements for Nonplanar Orbital Change with Continuous Propulsion With or Without Auxiliary Aerodynamic Forces. SSD-TDR-63-366, February 1964.

7. Bruce, R.W.: The Combined Aerodynamic-Propulsive Orbital Plane Change Maneuver. AIAA Paper 65-20, January 1965; also as SSD-TDR-64-98, June 1964.

8. Cuadra, E. and Arthur, P.D.: Orbit Plane Change by External Burning Aerocruise. AIAA Paper 65-21, January 1965.

9. Shaver, R.D.: Minimum Energy Loss Heading Changes for Hypersonic Flight from Orbit. The Rand Corp., RM-4391-PR, January 1965.

10. Bonin, L.J.: Impulse Required for Aerodynamic Plane Change of a Satellite Orbit. AIAA Paper 66-59, January 1966.

11. Parsons, W.D.: Analytic Solutions of the Synergetic Turn. J.S.R., vol. 3, pp. 1675-1678, November 1966.

12. Clauss, J.S., Jr., and Yeatman, R.D.: Effect of Heating Restraints on Synergetic Maneuver Performance. J.S.R., vol. 4, pp. 1107-1109, August 1967; also as AIAA Paper 67-169.

13. Lau, J.: Implications of Maneuvering-Range Constraints on Lifting-Vehicle Design. J.S.R., vol. 4, pp. 639-643, May 1967.

14. Paine, J.P.: Use of Lifting Re-Entry Vehicles for Synergetic Maneuvers. J.S.R., vol. 4, pp. 698-700, May 1967.

15. Tramonti, L.: The Effect of Finite Thrust on the Synergetic Plane Change: In Saturn V/Apollo and Beyond; National Symposium, Huntsville, Ala., June 11-14, 1967, Transactions, vol. 2, A 68-16783 05-30, Edited by S.S. Hu, Tarzana, Calif., American Astronautical Society, 1967, 25 pp., 11 Ref.

REFERENCES (Concluded)

16. Maslen, S.H.: Synergetic Turns with Variable Aerodynamics. J.S.R., vol. 4, pp. 1475-1482, November 1967.

17. Roessler, M.: Optimal Aerodynamic-Propulsive Maneuvering for the Orbital Plane Change of a Space Vehicle. J.S.R., vol. 4, pp. 1678-1680, December 1967.

18. Bonner, M.M.: Minimum Fuel Trajectories for the Synergetic Plane Change Maneuver. Ph.D. Thesis, Michigan University, Ann Arbor, 1967.

19. Dickmanns, E.D.: Gesteuerte Drehung von Satellitenbahnen durch Eintauchen in die dichtere Atmosphare. Ph.D. Thesis, RWTH Aachen, Germany, 1969, Also DFVLR-Sonderdruck, no. 42.

20. Dickmanns, E.D.: Optimal Control for Synergetic Plane Change. Paper presented at the Twentieth IAC, Mar del Plata, Argentina, 1969.

21. Schadt, G.H.: Aerodynamic Heating Problems With and Their Influence on Earth Orbit Lifting Entry Spacecraft. AIAA Paper no. 68-1126, October 1968.

22. Dash, M.J.: MDAC Orbiter Temperature Boundaries. Memo S&E-AERO-AT-71-22, November 30, 1971.

23. Bryson, A.E., Jr., Denham, W.F., and Dreyfus, S.E.: Optimal Programming Problems with Inequality Constraints. I: Necessary Conditions for Extremal Solutions. AIAA J., vol. 1, 11, pp. 2544-2550. November 1963.

24. Keller, H.B.: Numerical Methods for Two-Point Boundary Value Problems. London, Blaisdell, 1968.

25. Bulirsch, R.: Die Mehrzielmethode zur numerischen Lösung von nichtlinearen Randwertproblemen. Lehrgang Flugbahnoptimierung, Carl-Cranz-Gesellschaft e.V., West Germany, 1971.

26. Stoer, J., Bulirsch, R.: Einführung in die Numerische Mathematik II. Heidelberger Taschenbücher HT 114, Springer Verlag, 1973, pp. 170-191.

NASA-Langley, 1973 — 31 M105

"The aeronautical and space activities of the United States shall be conducted so as to contribute . . . to the expansion of human knowledge of phenomena in the atmosphere and space. The Administration shall provide for the widest practicable and appropriate dissemination of information concerning its activities and the results thereof."

—NATIONAL AERONAUTICS AND SPACE ACT OF 1958

NASA SCIENTIFIC AND TECHNICAL PUBLICATIONS

TECHNICAL REPORTS: Scientific and technical information considered important, complete, and a lasting contribution to existing knowledge.

TECHNICAL NOTES: Information less broad in scope but nevertheless of importance as a contribution to existing knowledge.

TECHNICAL MEMORANDUMS: Information receiving limited distribution because of preliminary data, security classification, or other reasons. Also includes conference proceedings with either limited or unlimited distribution.

CONTRACTOR REPORTS: Scientific and technical information generated under a NASA contract or grant and considered an important contribution to existing knowledge.

TECHNICAL TRANSLATIONS: Information published in a foreign language considered to merit NASA distribution in English.

SPECIAL PUBLICATIONS: Information derived from or of value to NASA activities. Publications include final reports of major projects, monographs, data compilations, handbooks, sourcebooks, and special bibliographies.

TECHNOLOGY UTILIZATION PUBLICATIONS: Information on technology used by NASA that may be of particular interest in commercial and other non-aerospace applications. Publications include Tech Briefs, Technology Utilization Reports and Technology Surveys.

Details on the availability of these publications may be obtained from:

SCIENTIFIC AND TECHNICAL INFORMATION OFFICE

NATIONAL AERONAUTICS AND SPACE ADMINISTRATION

Washington, D.C. 20546